

Site M0061¹

T. Andrén, B.B. Jørgensen, C. Cotterill, S. Green, E. Andrén, J. Ash, T. Bauersachs, B. Cragg, A.-S. Fanget, A. Fehr, W. Granoszewski, J. Groeneveld, D. Hardisty, E. Herrero-Bervera, O. Hyttinen, J.B. Jensen, S. Johnson, M. Kenzler, A. Kotilainen, U. Kotthoff, I.P.G. Marshall, E. Martin, S. Obrochta, S. Passchier, N. Quintana Krupinski, N. Riedinger, C. Slomp, I. Snowball, A. Stepanova, S. Strano, A. Torti, J. Warnock, N. Xiao, and R. Zhang²

Chapter contents

Introduction	1
Operations	1
Lithostratigraphy	2
Biostratigraphy	3
Geochemistry	6
Physical properties	8
Paleomagnetism	8
Microbiology	10
Stratigraphic correlation	10
References	11
Figures	13
Tables	35

Introduction

During Integrated Ocean Drilling Program (IODP) Expedition 347, cores were recovered from three holes at Site M0061 (Ångermanälven River estuary), with an average site recovery of 97%. In addition, three shallow gravity (Rumohr) cores were acquired. The water depth was 87.9 m, with no tidal range. Existing data sets, including seismic reflection profiles, were evaluated prior to each site to attempt to guide the initial drilling with an anticipated lithologic breakdown. The total time spent on station was 1.23 days.

Operations

Transit to Hole M0061A

The *Greatship Manisha* left Site M0060 at 1030 h on 1 October 2013, on route to Site M0061 (proposed Site BSB-10) via Øresund. At 1400 h, the vessel slowed while a small crew vessel came alongside to deliver drill supplies and offload microbiology “live” samples. A pilot boarded the *Greatship Manisha* at 0755 h on 4 October, guiding the vessel through the Ångermanälven River estuary, arriving at Hole M0061A by 1000 h.

Hole M0061A

Operations commenced as soon as the vessel had established position and built the dynamic positioning (DP) model (Table T1). Ten piston cores were recovered to deck before the evening of 4 October 2013. Initially, seawater was used for pumping, but because of the presence of sand, Guar gum drill mud was used deeper than 20.0 meters below seafloor (mbsf). At 2220 h, a hammer sample was collected, which retrieved a sample of granite. The hole was terminated at 25.20 mbsf at 2300 h on 4 October.

A total of 11 coring attempts were made in Hole M0061A to a maximum depth of 25.20 mbsf. Hole recovery was 94.87%.

Hole M0061B

The vessel moved to establish position for Hole M0061B under DP. At 2340 h, operations commenced with the first core recovered to deck at 0000 h on 5 October 2013.

¹Andrén, T., Jørgensen, B.B., Cotterill, C., Green, S., Andrén, E., Ash, J., Bauersachs, T., Cragg, B., Fanget, A.-S., Fehr, A., Granoszewski, W., Groeneveld, J., Hardisty, D., Herrero-Bervera, E., Hyttinen, O., Jensen, J.B., Johnson, S., Kenzler, M., Kotilainen, A., Kotthoff, U., Marshall, I.P.G., Martin, E., Obrochta, S., Passchier, S., Quintana Krupinski, N., Riedinger, N., Slomp, C., Snowball, I., Stepanova, A., Strano, S., Torti, A., Warnock, J., Xiao, N., and Zhang, R., 2015. Site M0061. In Andrén, T., Jørgensen, B.B., Cotterill, C., Green, S., and the Expedition 347 Scientists, *Proc. IODP, 347*: College Station, TX (Integrated Ocean Drilling Program).

doi:10.2204/iodp.proc.347.105.2015

²Expedition 347 Scientists' addresses.

At 0506 h, the tool became stuck. Following release of the overshot and flushing, the tool was freed and coring continued.

Nine piston cores were recovered during the morning of 5 October, reaching a maximum depth of 28.70 mbsf. As with Hole M0061A, the recovery of sand and silt led to the termination of the hole, and the vessel prepared to move to Hole M0061C at 0645 h on 5 October.

A total of nine coring attempts were made in Hole M0061B, reaching a maximum depth of 28.70 mbsf. Hole recovery was 97.98%.

Hole M0061C

Piston coring operations in Hole M0061C commenced at 0725 h on 5 October 2013, after the vessel had bumped across under DP. This hole was cored to produce a composite record with the previous holes and ensure an appropriate volume of material was collected to meet future sampling requirements. Consistent with Holes M0061A and M0061B, the hole was terminated upon encountering the sand lithology beneath the varved sequence.

A total of seven piston coring attempts were made in Hole M0061C, reaching a depth of 23.1 mbsf. Hole recovery was 98.4%.

Holes M0061K, M0061L, and M0061M

Three Rumohr cores were also collected at this site on 5 October 2013. The corer was deployed over the starboard side of the vessel using a system of winches. In total, 0.97 m (Hole M0061K), 0.96 m (Hole M0061L), and 0.92 m (Hole M0061M) of sediment was recovered in the attempt to capture the sediment/water interface without disturbance from the landing of the seabed template.

Lithostratigraphy

Six holes were drilled at Site M0061: Hole M0061A to a total depth of 25.2 mbsf, Hole M0061B to 28.7 mbsf, and M0061C to 23.1 mbsf. Holes M0061K–M0061M were Rumohr cores (<1 m penetration gravity cores) designated for microbiology and paleoceanographic sampling. The Rumohr cores were not included in the core description at the IODP Bremen Core Repository (Germany).

Piston coring was the primary coring method used in Holes M0061A–M0061C, with the exception of the bottom of Hole M0061A, where it became difficult to retrieve core as the sediment became sandier and coring changed to hammer sampling. At the base of that hole, a hard layer was reached where only a

granite rock ~5 cm in diameter was recovered (see “[Operations](#)”). The cores are slightly to moderately disturbed, and in Unit IV, the sediment was waterlogged and deformed, which prevented the clear identification of internal structures. Lithostratigraphic subdivisions are based on descriptions on the cut face of the split core from Hole M0061A with a core recovery of nearly 95% and supplemented by information from Holes M0061B and M0061C. Because of time constraints, only a small number of smear slides from core catchers were examined, and the data should be treated with caution because of core disturbance and contamination affecting core catcher material in general.

Site M0061 is divided into four lithostratigraphic units (Fig. [F1](#)). Unit I (0–2.30 mbsf; Hole M0061A) is composed of greenish black organic-rich clay influenced by expanding methane. A gradual transition is observed to Unit II, which is divided into Subunit IIa (2.30–6.46 mbsf; Hole M0061A), a dark greenish gray weakly varved clay with weak sulfide banding, Subunit IIb (6.46–6.90 mbsf; Hole M0061A), a downhole continuation of Subunit IIa dominated by black laminae rich in iron sulfide, and Subunit IIc (6.90–8.10 mbsf; Hole M0061A), which is gray clay. Unit III (8.10–14.50 mbsf; Hole M0061A) is dark greenish gray clayey silt with a varvic, rhythmic lamination that gradually grades to the dark gray silty sand and fine sands of Unit IV (14.50–28.70 mbsf; Hole M0061B). Unit IV also contains limited numbers of dispersed pebble-sized clasts.

Unit I

Intervals: 347-M0061A-1H-1, 0 cm, to 2H-1, 80 cm; 347-M0061B-1H-1, 0 cm, to 1H-2, 90 cm; 347-M0061C-1H-1, 0 cm, to 1H-2, 94 cm

Depths: Hole M0061A = 0–2.30 mbsf; Hole M0061B = 0–2.40 mbsf; Hole M0061C = 0–2.44 mbsf

Unit I is chiefly composed of a greenish gray to black clay that is only slightly disturbed with good recovery. The uppermost 40 cm is mostly greenish gray, becoming blacker downhole, marking increasing organic matter contribution. The clay comprises weak lamination, with millimeter-scale black laminae and spots, often smeared as a result of the core splitting process. Possible bioturbation is present at some intervals but is often very faint. The clay is very well sorted, with small voids due to methane expansion dispersed along the upper half of the unit especially. Smear slide studies (see “[Core descriptions](#)”) show that the terrigenous components consist of 90% silt and only 5% sand, as well as clay with a composition dominated by quartz, limited feldspar, and traces of biotite.

Black organic-rich clay with indistinct varves likely signifies deposition in conditions similar to a brackish-marine environment. Visible black banding is likely due to diagenetic sulfidization linked to organic accumulation during events of lower oxygen content.

Unit II

Subunit IIa

Intervals: 347-M0061A-2H-1, 80 cm, to 3H-2, 16 cm; 347-M0061B-1H-2, 90 cm, to 3H-1, 20 cm; 347-M0061C-1H-2, 94 cm, to 3H-1, 90 cm

Depths: Hole M0061A = 2.30–6.46 mbsf; Hole M0061B = 2.40–6.30 mbsf; Hole M0061C = 2.44–7.50 mbsf

Subunit IIb

Intervals: 347-M0061A-3H-2, 16 cm, to 3H-2, 60 cm; 347-M0061B-3H-1, 20 cm, to 3H-1, 70 cm; 347-M0061C-3H-1, 90 cm, to 3H-1, 1.40 cm

Depths: Hole M0061A = 6.46–6.90 mbsf; Hole M0061B = 6.30–6.80 mbsf; Hole M0061C = 7.50–8.00 mbsf

Subunit IIc

Intervals: 347-M0061A-3H-2, 60 cm, to 4H-1, 0 cm; 347-M0061B-3H-1, 70 cm, to 3H-2, 30 cm; 347-M0061C-3H-1, 1.40 cm, to 3H-2, 64 cm

Depths: Hole M0061A = 6.90–8.10 mbsf; Hole M0061B = 6.80–7.89 mbsf; Hole M0061C = 8.00–8.74 mbsf

The upper part of the unit consists of dark greenish gray silty-sandy organic-rich clay with weak gray lamination on millimeter scales, often in 2–5 cm bundles. Sparse bioturbation is observed, and the sediment is very well sorted. In Subunit IIb, black iron sulfide laminae dominate (Fig. F2). Subunit IIc is a lithologic continuation of the clay in Subunits IIa and IIb, but gray and without the presence of iron sulfide. Smear slide studies (see “[Core descriptions](#)”) show that the terrigenous components consist of 90% sand and 10% silt with a composition dominated by quartz and feldspar and minor contents of biotite.

This fine laminated silty clay with high organic content is interpreted as possible annual sediment laminae (varves) deposited in a localized protected basin. The rhythmic appearance possibly reflects local climatic changes in organic matter accumulation. The black laminated horizon represents increased iron sulfide diagenetic processes within Subunit IIb. This increase may represent periods of low oxygen and increased organic matter deposition, providing sufficient conditions for sulfide formation. The lower-

most part (Subunit IIc) is a transition zone in the generally lithologically normal graded fjord sediments.

Unit III

Intervals: 347-M0061A-4H-1, 0 cm, to 7H-1, 0 cm; 347-M0061B-3H-2, 30 cm, to 5H-2, 30 cm; 347-M0061C-3H-2, 64 cm, to 5H-2, 50 cm

Depths: Hole M0061A = 8.10–14.5 mbsf; Hole M0061B = 7.89–14.50 mbsf; Hole M0061C = 8.74–15.20 mbsf

Unit III comprises dark greenish gray interlaminated clayey silt and silt, rhythmites, and perhaps varves fining upward within one lamina (silt to clay); lamination is visible by changes in grain size and color with a general thickness of laminae around 1–4 cm. The unit is very well sorted and slightly disturbed, gradually grading downhole to the sand of Unit IV.

This fine laminated silty sediment is interpreted as annual sediment laminae (varves) deposited in a locally protected basin. The rhythmic appearance possibly reflects local climatic changes.

Unit IV

Intervals: 347-M0061A-7H-1, 0 cm, to end of hole; 347-M0061B-5H-2, 30 cm, to end of hole; 347-M0061C-5H-2, 50 cm, to end of hole

Depths: Hole M0061A = 14.50–25.2 mbsf; Hole M0061B = 14.50–28.7 mbsf; Hole M0061C = 15.20–23.10 mbsf

Unit IV consists of dark gray homogeneous silty sand with clayey silt interbeds on a centimeter scale, grading downhole to medium, washed sand containing brown specks (small plant remnants, opaques, and white mica). Grain shapes are subangular to subrounded. A few dispersed gravel clasts are present.

The downhole increase of sand and rare gravel-sized clasts may be evidence for a glacially influenced environment, possibly influenced by meltwater flow.

Biostratigraphy

Diatoms

Qualitative analyses for siliceous microfossils were carried out on 21 samples from Hole M0061A and 4 samples from Hole M0061B with an interval of 1.5 to 3 m between samples. Diatoms were identified to species level, and ebridians and chrysophyte cysts were recorded if present. The results of the qualitative diatom analyses for both holes are summarized in graphs showing the number of taxa found, divided into different salinity affinities and life forms (planktonic, periphytic, and sea ice) (Figs. F3, F4).

The occurrence of diatom taxa in studied samples is shown in Tables T2 and T3. A species list of all 97 recorded taxa from Site M0061 is presented in Table T4. Diatoms were classified with respect to salinity tolerance according to the Baltic Sea intercalibration guides of Snoeijs et al. (1993–1998), which divide taxa into five groups: marine, brackish-marine, brackish, brackish-freshwater, and freshwater. The preservation in all slides containing diatoms can be considered good with lightly siliceous taxa still present. Chrysophyte cysts of various morphotypes were present in all slides where diatoms were recorded.

0 to ~2 mbsf

The assemblage recorded in this interval reflects a dynamic brackish estuary environment with large river input. The uppermost interval recorded in Hole M0061A has a relatively diverse assemblage (Fig. F3). It is a mixture of freshwater taxa (e.g., periphytic *Tabularia flocculosa*, *Fragilaria exigua*, *Eunotia implicata*, and planktonic species from the genera *Aulacoseira* and *Cyclotella*), brackish-freshwater taxa (e.g., periphytic *Rhopalodia gibba*, *Epithemia sorex*, *Epithemia turgida*, *Cocconeis pediculus*, and planktonic *Thalassiosira baltica*), and brackish taxa (e.g., periphytic *Rhoicosphenia curvata* and planktonic *Pauliella taeniata* and *Thalassiosira levanderi*). The freshwater taxa in this uppermost interval probably reflect allochthonous river input from Ångermanälven River. The influence of sea ice taxa is observed in this sequence, consisting of *P. taeniata*, *Fragilariopsis cylindrus*, and *Melosira arctica*. *P. taeniata* is an Arctic planktonic sea ice diatom abundant in the entire Baltic Sea area that dominates the spring bloom after cold winters with extensive ice cover (Hajdu et al., 1997; Hasle and Syvertsen, 1990; Snoeijs, 1993–1998; Weckström and Juggins, 2006).

~2–6 mbsf

The diatom assemblage in this interval indicates a brackish water, open-coastal environment with some influence from fluvial input. It was only recorded in one sample from Hole M0061A (4.8 mbsf), so four additional samples from Hole M0061B (2.8–6.1 mbsf) were analyzed to cover this interval (Figs. F3, F4). The assemblage is dominated by brackish (e.g., planktonic *Thalassiosira hyperborea* var. *lacunosa*, *T. levanderi*, *Cyclotella choctawhatcheeana*, *P. taeniata*, and periphytic *R. curvata* and *Cocconeis scutellum*) and brackish-marine taxa (e.g., *Tabularia fasciculata*) but also some marine taxa, especially in the lowermost part (e.g., *Pseudosolenia calcar-avis* and *Opephora marina*). Brackish-marine *Chaetoceros* spp. resting spores are common throughout the sequence. There is also a constant record of ~10%–25% freshwater di-

atom taxa most probably reflecting transported river input. The ebridian *Ebria tripartita* is recorded at all analyzed levels.

~6–8 mbsf

The diatom assemblage at this interval suggests a freshwater (large lake) environment with weak influence of brackish water. The transition from this assemblage (recorded at 6.3 mbsf in Hole M0061A) to a brackish environment (recorded at 6.1 mbsf in Hole M0061B) is not defined and must be investigated further. The sequence was recorded in three samples from Hole M0061A, and the assemblage is dominated by freshwater taxa (e.g., the large lake taxa *Stephanodiscus neoastreae*, *Aulacoseira islandica*, *Gomphocymbella ancylii*, and *Cocconeis disculus* [Hedenström and Risberg, 1999]), but brackish-freshwater ice algae *Fragilariopsis cylindrus* was also common in the uppermost sample (6.3 mbsf) (Fig. F3).

9.6 mbsf to bottom of core

This interval is more or less barren of siliceous microfossils; only single frustules and fragments of diatoms and one Chrysophyte cyst were found (Fig. F3).

Foraminifers

Results are summarized for the samples taken offshore and onshore (i.e., samples taken from core catchers and regular sections). A total of 50 samples were processed and scanned from Holes M0061A, M0061B, and M0061C for the presence of foraminifers (Table T5). Foraminifers were previously not recorded for the Bothnian Sea and its estuaries. This is possibly due to the very low salinity in this part of the Baltic Sea, as bottom water salinity in the Ångermanälven River estuary is around 5 (Samuelsson, 1996). Past reconstructions of salinity based on Sr isotopes of mollusk shells suggested that during the middle Holocene salinity might have been as high as 10–12 in the Bothnian Sea, allowing a foraminiferal community to become established (Widerlund and Andersson, 2011).

Site M0061 cores contain significant benthic foraminifers for selected samples (Fig. F5). All foraminifers belong to a single species, *Elphidium albiumbilicatum*. *E. albiumbilicatum* is able to survive under very low salinity conditions (Rottgardt, 1952; Lutze, 1965). Foraminifers are found between 1.69 and 6.23 mbsf with a maximum abundance classified as “common” in the core catcher sample from Core 347-M0061C-1H (Fig. F5). The occurrence of foraminifers at Site M0061 can potentially be linked to the slightly higher salinity conditions that are reconstructed for the middle Holocene (Widerlund and

Andersson, 2011). However, foraminifers were not present in every sample in this interval. This might be related to a combination of the dynamic setting within the estuary and the low salinity such that conditions were not continuously appropriate for foraminifers to form a population. As such, the presence of foraminifers is only appointed to specific samples instead of to a certain interval.

Ostracods

Ostracods were examined from 49 samples (including 23 core catchers) from Holes M0061A, M0061B, and M0061C during the onshore phase of Expedition 347 at the Bremen Core Repository. Samples were studied in the >125 μm fraction. Ostracods were present in eight samples (Table T6).

Ostracod abundance per sediment volume from the three holes was low and is shown in Figure F6. Four species were identified: *Hirschmania viridis*, *Paracyprideis fennica*, *Sarsicytheridea punctillata*, and *Heterocyprideis sorbyana*.

P. fennica is the most common species at this site, occurring in the interval 0.17–4.45 mbsf (Holes M0061A–M0061C). Deeper, at 5.11 mbsf (Core 347-M0061A-3H-1, 30–32 cm), only one species, *H. viridis*, was recorded. The interval immediately deeper, to 28.68 mbsf (Holes M0061A–M0061C), was barren. Similarly, foraminifers were only found from 1.69 to 6.23 mbsf (see “Foraminifers”). The highest number of ostracods was recorded at 2.82 mbsf (Hole M0061B) (Table T6) in the only sample where *S. punctillata* and *H. sorbyana* were recorded.

Such low abundance and taxonomic diversity implies harsh environments for ostracods. *P. fennica*, *S. punctillata*, and *H. sorbyana* are all known to tolerate a wide range of salinities from 4 to fully marine conditions; *P. fennica* can also be found in low-oxygen environments (Frenzel et al., 2010). Low salinity is not a limiting factor for ostracod abundance, as many taxa tolerate fresh and brackish water environments, but similarity between ostracod and foraminifer records implies that salinity decreases toward the uppermost samples. Another important factor is the very high sedimentation rates that decrease in the upper part of the record (see “Lithostratigraphy”), allowing microfossils to be preserved.

Palynological results

For Site M0061, palynological analyses focused on Hole M0061B. Generally, one sample per core was examined for palynomorphs. Today, the regional vegetation in the terrestrial area around Site M0061 is dominated by pine (*Pinus*), birch (*Betula*), and

spruce (*Picea*) trees and belongs to the boreal-forest vegetation zone with taiga-like conditions.

Nine sediment samples were analyzed from Hole M0061B. The uppermost four samples contained enough palynomorphs to get statistically relevant results (Figs. F7, F8). Bisaccate pollen was included in the reference sum, but at least 50 nonsaccate pollen grains were counted per sample in order to cope with the high percentages of bisaccate pollen.

0.13–6.62 mbsf

Pollen concentrations are between $\sim 40,000/\text{cm}^3$ and $\sim 180,000/\text{cm}^3$ in the four samples analyzed from this interval (see PalyM0061.xls in PALYNOLOGY in “Supplementary material”). *Pinus* is the dominant pollen taxon in all samples. The second most frequent pollen type in most samples is *Betula* pollen. The two uppermost samples analyzed show some difference compared to the two deeper samples. *Picea* (spruce) pollen shows percentages up to 17% in the two uppermost samples (0.13 and 1.53 mbsf; Fig. F7). It is accepted that spruce arrived at the Swedish-Bothnian coast around 3500 cal y BP (Huntley and Birks, 1983; Segerström and von Stedingk, 2003). This would imply that the age of the sample at 1.53 mbsf dates to at least 3500 y BP. Worthy of mention here is the presence of *Betula nana* pollen, a dwarf birch growing under arctic and cool temperate climatic conditions (for instance, central and northern Sweden). The two uppermost samples are also characterized by the high-frequency presence of *Radioispermia corbiferum* (Fig. F8), a dubious taxon which has so far been described as an acritarch, mollusk egg, or algal cyst (also called “Sternhaarstatoplast,” e.g., Nehring, 1994). *Picea* is virtually absent in the deeper samples from this interval (4.42 and 6.26 mbsf). In some samples, pteridophyte spores are also common, with recurrent presence of *Dryopteris* (wood fern), particularly in the sample from 6.26 mbsf. Dinocysts and other marine palynomorphs were extremely rare in these samples, except for one sample at 4.42 mbsf that contained several specimens of *Operculodinium centrocarpum*/*Protoceratium reticulatum*. All of them have particularly short processes, which may indicate low salinity (Mertens et al., 2009). This finding is congruent with foraminifer-based results, which indicate a slightly stronger marine influence between 3.40 and 4.90 mbsf indicated by slightly increased abundances of foraminifers (genus *Elphidium*) and lower frequency/absence of foraminifers shallower than these depths. Generally, the rarity of marine taxa in this interval points to a strong terrestrial influence, with particularly low influence in the upper samples.

13.0–26.15 mbsf

Five samples from this interval were analyzed, but none of them contained enough pollen to generate statistically relevant results. Most samples were completely barren of palynomorphs. This is in accordance with sedimentological findings, which indicate that the samples originate from silty/sandy sediments. Thus, palynomorphs either occur in very low concentration in this material or were completely degraded because of oxidation.

Geochemistry

At Site M0061, silty and sandy sediments are overlain by ~8 m of clays (see “[Lithostratigraphy](#)”). The geochemical concentration profiles at Site M0061 reflect strong variations in depositional conditions in the outer Ångermanälven River estuary.

Interstitial water

Salinity variations: chloride, salinity, and alkalinity

Chloride (Cl^-) concentrations are lowest at the top of the profile with values around 100 mM and increase to ~130 mM at 8 mbsf (Fig. [F9A](#)). Deeper concentrations are almost constant with a slight decrease of 3–4 mM between 15 and 20 mbsf. Shipboard salinity measured with a refractometer ranges ~6–10 and shows the same general depth trend as Cl^- based salinity (Fig. [F9B–F9C](#)). Shipboard salinity values for Hole M0061C are higher than those for Holes M0061A and M0061B; however, Cl^- based salinities for all holes are very similar (Fig. [F9C](#); Table [T7](#)). The salinity concentration profiles show freshwater impact in the surface sediments, likely related to fluvial input.

Alkalinity increases from 13.5 meq/L in the uppermost sample to ~20 meq/L at 5.5 mbsf followed by a gradual decrease to ~6 meq/L at the core bottom (Fig. [F9D](#)).

Organic matter degradation: sulfate, sulfide, ammonium, phosphate, iron, manganese, pH, bromide, and boron

Sulfate (SO_4^{2-}) concentrations from Hole M0061C remain <0.25 mM until ~16 mbsf, where there is a gradual increase to 2.8 mM at 21 mbsf (Fig. [F10A](#)). In Holes M0061A and M0061B, SO_4^{2-} concentrations remain below detection until ~21 mbsf and then gradually rise to 3.8 mM by 27 mbsf. The overall similarity of the SO_4^{2-} profiles of the three holes suggest

that contamination by drilling fluid is probably negligible and the measured SO_4^{2-} in the deeper sediment intervals may be provided by a subsurface source or a lateral inflow of sulfate-rich waters into the sandy deposits (see “[Lithostratigraphy](#)”).

Pore water sulfide (H_2S) was detected only in the uppermost sediment sequence (<8 mbsf) with values not exceeding 5 μM (Fig. [F10B](#)). The downhole trend in ammonium (NH_4^+) is similar to that of alkalinity (Fig. [F10C](#)). Values increase from 0.5 mM in the uppermost sample to a maximum value of 1.3 mM at ~6 mbsf before gradually decreasing downhole to 0.24 mM by 27 mbsf. The phosphate (PO_4^{3-}) concentration profile shows an increase from 0.4 mM in the uppermost sample to a peak of 0.6 mM by 2.5 mbsf (Fig. [F10D](#)). Deeper than this maximum, concentrations slowly decline to values of 1–2 mM by ~8–10 mbsf and below detection by 22 mbsf. These results indicate high rates of organic matter degradation in the upper ~8 m of the core.

Dissolved iron (Fe^{2+}) and manganese (Mn^{2+}) concentrations are elevated near the sediment surface (95 and 250 μM , respectively), followed by a zone of depletion with the lowest values around 5 mbsf for both cations (Fig. [F10E–F10F](#)). Iron concentrations then increase to ~350 μM by 12 mbsf, followed by a gradual decrease to <100 μM at the bottom of the profile. Manganese concentrations gradually rise to ~120 μM by 15 mbsf and then decline to ~60 μM at 27 mbsf.

pH is characterized by some variation in the uppermost sediment sequence (<8 mbsf) but generally shows similar trends between holes (Fig. [F10G](#)). There is an increase from 7.8 in the uppermost sample to a peak of ~8 between 6 and 8 mbsf. Deeper pH values decline to near 7.6 by 12 mbsf and remain fairly constant for the remainder of the sampled interval.

The profile for bromide (Br^-) largely follows the salinity profile with an increase from 0.16 to 0.21 mM in the upper 6–7 mbsf. Deeper Br^- concentrations show little variation downcore (Fig. [F11A](#)). There are only small variations in the Br/Cl ratio (Fig. [F11B](#)). The low Br^- concentrations together with low alkalinity values suggest low rates of organic matter degradation at this site. Boron (B) concentrations show a maximum of ~140 μM at ~4 mbsf, followed by a decrease downhole and the absence of B deeper than ~20 mbsf (Fig. [F11C](#)). The B/Cl ratio is elevated above the seawater ratio and peaks at 4 mbsf, and then the ratio drops gradually to approach zero deeper than ~20 mbsf (Fig. [F11D](#)).

Mineral reactions

Sodium, potassium, magnesium, and calcium

Sodium (Na^+), potassium (K^+), and magnesium (Mg^{2+}) concentrations all increase with depth in the upper 5–8 mbsf (Fig. F12A–F12C). Deeper concentrations of Na^+ and K^+ gradually decline to ~75 and 1.3 mM, respectively, toward the base of the profile. Magnesium concentrations increase from 9 mM at the top to ~13 mM at 5 mbsf, decrease to 10 mM at 15 mbsf, and then rise again to ~13 mM at the bottom of Holes M0061A and M0061B. Note that Mg^{2+} concentrations remain near constant in the lower part of Hole M0061C (Fig. F12C). Calcium (Ca^{2+}) concentrations increase steadily with depth from ~2.3 in the upper section to ~24 mM at 27 mbsf (Fig. F12D). The ratios of Na/Cl and K/Cl indicate that both Na^+ and K^+ are depleted relative to seawater ratios in sediments deeper than ~10 mbsf (Fig. F12E–F12F). Mg/Cl ratios are near constant (Fig. F12G), whereas those of Ca/Cl increase with depth (Fig. F12H). The high Ca^{2+} and Mg^{2+} concentrations between 10 and 22 mbsf in Hole M0061C compared to Holes M0061A and M0061B are not balanced by an equivalent concentration of anions. This suggests that the data for Hole M0061C should be viewed with caution.

The Ca^{2+} concentration profiles from all three holes clearly show release of Ca^{2+} from sediments. In combination with the Ca/Cl ratios, which display a gradual increase downcore, the Ca^{2+} data indicate a source of calcium in deeper subsurface sediments, including potential Ca^{2+} displacement from solid phases at depth by Na^+ and K^+ through ion exchange and/or dissolution of Ca-bearing phases.

Strontium, lithium, silica, and barium

The strontium (Sr^{2+}) concentration profile is similar to that of Ca^{2+} . Concentrations increase from 16 μM in the topmost pore water samples to 68 μM at the bottom of the profile (Fig. F13A).

Lithium (Li^+) concentrations increase from ~5 μM in the uppermost section to 8.6 μM near 5 mbsf (Fig. F13B). Deeper concentrations decrease to a value of ~3 μM at 9 mbsf and then increase again to an average value close to 10 μM at the base of the profile.

Dissolved silica (H_4SiO_4) concentrations are elevated in the upper 8 mbsf with a concentration near 700 μM (Fig. F13C). Deeper, there is an abrupt drop of H_4SiO_4 close to 340 μM . Concentrations remain constant for the remainder of the profile. This trend may

relate to a dissolution of diatoms, which are present in the upper 8 mbsf (see “[Biostratigraphy](#)”).

Barium (Ba^{2+}) concentrations increase with depth from 0.4 μM near the surface to ~15–20 μM around 15 mbsf (Fig. F13D). Deeper than this peak, values gradually decrease to the bottom of the profile. Hole M0061C again shows distinct variation from Holes M0061A and M0061B. The Ba^{2+} enrichment with depth may be explained by Ba^{2+} desorption, weathering reactions, or dissolution of barium-containing minerals, which is enhanced when interstitial water sulfate is low.

Molybdenum, vanadium, and titanium

Molybdenum (Mo) and vanadium (V) are highly variable in concentration with depth and between holes (Table T8). Mo concentrations are relatively constant (e.g., 0.04 μM) in the upper 10 mbsf, followed by a maximum value directly deeper (up to 0.15 μM) and a decline toward the base of the profile. V concentrations, in contrast, decrease from 0.18 μM near the surface to values <0.1 μM deeper than 10 mbsf. Dissolved titanium (Ti) concentrations show a small but distinct trend consistent between holes in the uppermost sediments (Table T8). Concentrations of ~0.23 μM are observed at the core top, followed by a constant decline to values <0.01 μM around 9 mbsf.

Sediment

Carbon content

Sedimentary total carbon (TC) values (Fig. F14A; Table T9) reach a maximum of ~2.6 wt% in the upper 4–5 mbsf and then decrease to values below 0.2 wt% at 10 mbsf. The total organic carbon (TOC) profile largely resembles the one of TC, indicating that the majority of carbon is organic (Fig. F14B). The content of total inorganic carbon (TIC) in these sediments is low throughout the sediment column, with only slightly elevated concentrations (up to 0.25 wt%) in the upper ~8 mbsf (Fig. F14C).

Sulfur content

Total sulfur (TS) concentrations (Fig. F14D) follow the trend of the TOC profile with a maximum value of 2.3 wt% at the depth of the TOC maximum (~4.5 mbsf). Contents of TS decrease to low values (<0.2 wt%) deeper than the maximum to ~8 mbsf and stay low downcore. The high TOC and TS concentrations coincide with black bands described in the clays of lithostratigraphic Subunit I1b (see “[Lithostratigraphy](#)”).

phy”) and are likely related to the presence of metal sulfide minerals in these sediment layers.

Physical properties

This section summarizes the preliminary physical property results from Site M0061. Three holes were drilled at this site. Hole M0061A was drilled to 25.2 mbsf, Hole M0061B to 28.7 mbsf, and Hole M0061C to 23.1 mbsf. Additionally, three Rumohr cores (Holes M0061K, M0061L, and M0061M; <1 m in length) were collected at this site to attempt to capture the water/sediment interface and the uppermost surface sediments. Physical property measurements were not performed for these Rumohr cores. For Holes M0061A, M0061B, and M0061C, all physical property measurements described in “Physical properties” in the “Methods” chapter (Andrén et al., 2015a) were conducted. As the discrete moisture and density (MAD) and *P*-wave measurements are few in number, our interpretations are based primarily on the shipboard multisensor core logger (MSCL) data from Hole M0061B, which had the greatest penetration.

Magnetic susceptibility and color reflectance

Magnetic susceptibility generally increases downcore with distinct variations noted at lithostratigraphic unit boundaries (Fig. F15). Values are relatively constant through Unit I, with a low-amplitude excursion at the Unit I/Subunit IIa boundary followed by a gradual decrease in the upper interval of Subunit IIa. Magnetic susceptibility then increases downcore in Subunit IIa before dropping to low values in Subunit IIb and returning to high values in Subunit IIc. Lithology is similar throughout Unit II. Therefore, the change in magnetic susceptibility likely reflects changing organic content (see “Lithostratigraphy”). Unit III is characterized by increasing magnetic susceptibility to the Unit IV boundary. Unit IV exhibits relatively constant values with some large excursions around 22 and 26 mbsf.

Color reflectance, in particular b^* , reflects downcore changes in lithology (Fig. F15). Unit I exhibits relatively low (more blue) values, whereas Subunit IIa exhibits higher (more yellow) values. Subunit IIb is distinguished by increased blue reflectance, whereas Subunit IIc is characterized by increased yellow reflectance. Units III and IV are generally yellowish in color.

Natural gamma ray, noncontact resistivity, and *P*-wave velocity

Both natural gamma ray (NGR) and noncontact resistivity (NCR) increase through Units I and II, reaching peak values in the upper interval of Unit III (Fig. F15). There is a sharp decrease in both physical properties at ~9 mbsf in Unit III. That change could be related to a suggested erosional horizon at around that level (see “Stratigraphic correlation”). Although NGR returns to high values in the middle portion of Unit III, NCR remains low to the bottom of the hole. A similar trend in NGR data is observed at nearby Site M0062, located in Ångermanälven River estuary (see “Physical properties” in the “Site M0062” chapter [Andrén et al., 2015b]). Low NCR may indicate high water content in the cores, which is consistent with *P*-wave velocities in Unit IV that vary around ~1500 m/s (speed in water). In the upper sections of Hole M0061B, low *P*-wave velocities in Subunit IIa are likely caused by pervasive cracks. Low *P*-wave velocity spikes in portions of Units III and IV appear to result from core liners that were not fully filled with sediment.

Density

Gamma density was measured at 1 cm intervals during the offshore phase of Expedition 347 (Fig. F16). Gamma density increases from the core top to the upper interval of Unit III then decreases abruptly at ~11 mbsf before increasing again and remaining relatively constant to the bottom of the hole. Discrete bulk density measurements conducted during the Onshore Science Party (OSP) correlate well with the shipboard measurements ($r^2 = 0.93$; Fig. F17).

Paleomagnetism

To fulfill the main objectives of the OSP paleomagnetic work, we carried out basic analyses of the natural remanent magnetization (NRM) and magnetic susceptibility of discrete specimens of known volume and mass magnetic susceptibility (see “Paleomagnetism” in the “Methods” chapter [Andrén et al., 2015a]). A total of 309 discrete samples were taken from Holes M0061A (128 samples), M0061B (53 samples), and M0061C (128 samples) according to the site splice, with a higher density of sampling in the upper 11.5 m. Magnetic susceptibility (χ) ranges between 0.1×10^{-6} and 1.4×10^{-6} m³/kg through the sequence, with the highest value found

at the boundary between Subunits IIb and IIa, which is characterized by black (iron sulfide) staining.

Most of the paleomagnetic pilot samples recovered from Units IV and III carried a relatively intense NRM that reached 380×10^{-3} A/m. This NRM was easily demagnetized and has low magnetic stability. In addition, this relatively coarse sand interval has very scattered inclinations, with an average close to 15° . At 11.5 meters composite depth (mcd) (in Unit III), the NRM intensity decreases and the inclination increases to approach a geocentric axial dipole (GAD) prediction. An interval of high NRM intensity at the boundary between Subunits IIb and IIa is associated with observations of iron sulfide precipitation. The majority of samples in the top part of Unit III and Units II and I carried normal polarity NRMs, with secular variations around the GAD prediction. Pilot samples with relatively high χ taken from Unit IV and up to the middle of Unit III (11.5 mcd) acquired gyroremanent magnetization (GRM) during alternating field (AF) demagnetization above 50 mT, and these samples are associated with inclinations that approach the GAD prediction of 74° . The acquisition of a GRM indicates the presence of authigenic greigite (Fe_3S_4), which is responsible for secondary chemical remanent magnetizations of strictly unknown age (Snowball, 1997). The upper 6 m (part of Subunit IIa and Unit I) contains inclination data that can be correlated to features in a regional master curve (Snowball et al., 2007), but these require independent corroboration.

Discrete sample measurements

A total of 309 discrete samples were obtained from Holes M0061A, M0061B, and M0061C. Samples were recovered at intervals of ~ 50 cm from within the site splice.

Magnetic susceptibility

The results of the magnetic analyses are shown in Figure F18. Magnetic susceptibility (χ), which was normalized to sample mass, predominantly ranges between 0.1×10^{-6} and 0.6×10^{-6} m³/kg, with one outlier at 1.4×10^{-6} m³/kg. Samples taken within Unit IV have χ values between 0.2×10^{-6} and 0.4×10^{-6} m³/kg. Overlying Unit III has relatively lower χ values that generally do not exceed 0.3×10^{-6} m³/kg, with the exception of some high values (0.6×10^{-6} m³/kg) around 9 and 11 mbsf. Unit II has variable χ , and Subunit IIb is characterized by values of $<0.2 \times 10^{-6}$ m³/kg. Unit I, which is organic-rich laminated clay, has χ values close to 0.2×10^{-6} m³/kg.

Sediment wet density and χ are positively related, although the majority of the data are from the upper

11.5 m because of the higher sampling density in the upper part of the sequence. One significant observation is that shallow positive ($<40^\circ$) and negative inclinations are associated with a wide range of NRM intensity.

Natural remanent magnetization and its stability

Results of the pilot sample demagnetization (Fig. F19) indicate that a low AF of 5 mT is sufficient to remove a weak viscous remanent magnetization (VRM). Three different responses to the sequential AF demagnetization are displayed by samples from Site M0061. Category 1 includes the samples from the relatively coarse grained Units IV and III, which lose 50% of their NRM intensity at alternating fields less than 15 mT, with a small residual component left at 40 mT. These samples subsequently acquired a gyroremanent magnetization (GRM) at field levels >60 mT, with the vector moving into a plane perpendicular to the last demagnetization axis. Category 2, which includes all other pilot samples except those in Unit I, is typified by a paleomagnetic vector that is smoothly demagnetized up to the maximum AF demagnetization level of 80 mT, with a vector that trends toward the origin of the orthogonal projection. Category 3 has a relatively high magnetic stability, with $>50\%$ of the NRM removed between 15 and 30 mT, which can indicate a narrow magnetic grain size distribution.

After removal of the viscous overprint, the NRM intensity of the samples recovered from Site M0061 lies between 0.07×10^{-3} and 380×10^{-3} A/m and there is a general positive relationship with χ (Fig. F18). It is notable that the NRM intensity of Unit I and the interval of distinct iron sulfide precipitation between Subunits IIb and IIa is particularly high relative to χ , which suggests a more efficient recording of the geomagnetic field than in the other units.

Paleomagnetic directions

The directions of the subsample paleomagnetic vectors are illustrated by the inclination data in Figure F18. The inclination data from Unit IV and the lower part of Unit III are scattered, with the majority of the inclination values on the positive side of the diagram. Only a few samples from these two units approach the GAD prediction for this site location. In contrast, the inclination data from Units I and II and the uppermost part of Unit III group closer to the GAD prediction, but there is a bias toward shallow inclinations, particularly between 10 and 9 mbsf. It is notable that the samples taken from the upper part of Unit IV and Unit III, which have high χ val-

ues, plot relatively far away from the GAD prediction. The variable magnetic properties and different categories of response to AF demagnetization, which include samples that acquire GRM, probably preclude using the paleomagnetic data for relative dating purposes in Units IV and III. In particular, pilot samples that acquire GRM are restricted to intervals with inclinations that are close to the GAD prediction. These samples probably contain a secondary chemical remanent magnetization (CRM) carried by authigenic greigite (Fe_3S_4), which is known to acquire GRM (Snowball, 1997). The time lag between sediment deposition and greigite precipitation is unknown and, therefore, the ability to use the paleomagnetic data at Site M0061 for relative dating purposes is most likely restricted to Unit I and the upper half of Unit II, shallower than 5 mbsf. The interval of high inclinations grouped around a depth of ~ 2 mcd may correspond to one of the late Holocene inclination features identified in the FENNOSTACK regional master curve (Snowball et al. 2007), such as ϵ^1 (~ 2650 cal y BP) or γ (1290 cal y BP).

Microbiology

A Rumohr core was obtained from Hole M0061K to sample the uppermost 0–1 m of sediment specifically for cell counts and for onshore microbiology (DNA extraction and analysis). Counts of microbial cells were made on board the ship by fluorescence microscopy only using acridine orange direct count (AODC).

A total of 13 sediment samples were counted for microbial cell numbers on the ship (Table T10) using epifluorescence microscope counting techniques. Microbial cell abundance was very high (Fig. F20), with a maximum of 5.41×10^9 cells/cm³ at 0.04 mbsf decreasing linearly to a minimum of 6.90×10^8 cells/cm³ at 0.92 mbsf. This represents approximately an eight-fold decrease in cell numbers over 88 cm. All cell counts of this hole, apart from the uppermost sample at 0.01 mbsf, were very high, with all data values above the upper prediction limit of the global regression of prokaryote cells with depth.

Stratigraphic correlation

At Site M0061, three holes were drilled: M0061A (25.2 mbsf), M0061B (28.7 mbsf), and M0061C (23.1 mbsf). The meters composite depth scale for Site M0061 is based on the correlation of magnetic susceptibility between holes (Fig. F21). Shipboard Fast-track magnetic susceptibility measurements obtained from every other core were used to determine

the offset between adjacent holes (see “Physical properties”). These data provided an efficient tool to monitor and adjust the drilling process in order to maintain an adequate core overlap. All core material was also logged with a standard MSCL to enable more precise hole-to-hole correlation and to construct a composite section for Site M0061 (Fig. F21). Before analysis/correlation, all magnetic susceptibility data were cleaned to remove instrumental outliers. The depth offsets that define the composite section for Site M0061 are given in Table T11 (affine table).

Correlation between the susceptibility anomalies/data in Holes M0061A, M0061B, and M0061C is good, and it was possible to produce a continuous splice record for this site (Table T12). The splice was constructed mainly from Holes M0061A and M0061C. Hole M0061B was used in the splice to cover larger gaps at 8.5–10 and 14.2–15.3 mcd and in the lowermost part of the splice.

Accuracy of correlation was visually checked from scanned core slab images using the Corelyzer software. At Site M0061, correlation was straightforward to 25 mcd. The lowermost ~ 3 m of sand lacked distinctive MSCL data or sedimentological features to validate the correlation. A correction for either compression or expansion was not applied to the data, so offsets within each core were equal for all points. Therefore, it is possible that some features are not similarly aligned between holes.

Seismic units

Seismic sequence boundary-sediment core-MSCL log (magnetic susceptibility) correlations are shown in Figure F22. Correlations are based on the integration of seismic data and lithostratigraphy (see “Lithostratigraphy”). Two-way traveltime values were calculated for each lithostratigraphic unit boundary using sound velocity values measured offshore and during the OSP (see “Physical properties”; Table T13). Lithostratigraphic unit boundaries were examined at the calculated two-way traveltime values to define the extent of agreement between seismic boundaries and actual lithologic transitions and physical properties disconformable surfaces. Uncertainties in the time-depth function may have resulted in minor inconsistencies between seismic features, sedimentological observations from cores, and MSCL logs.

Seismic Unit I

Two-way traveltime: 0.123 ms

Lithology: greenish gray to black clay (lithostratigraphic Unit I)

Depths: Hole M0061A = 0–2.30 mbsf, Hole M0061B = 0–2.40 mbsf, Hole M0061C = 0–2.44 mbsf

The Unit I base matches the first clear boundary within a transparent and stratified seismic unit. It is also evident in physical properties, such as low magnetic susceptibility values, measured in sediment cores.

Seismic Unit II

Two-way traveltime: 0.131 ms

Lithology: dark greenish gray weakly varved clay with weak sulfide banding (lithostratigraphic Subunit IIa); iron sulfide-rich gray clay (lithostratigraphic Subunit IIb); and gray clay (lithostratigraphic Subunit IIc)

Depths: Hole M0061A = 2.30–8.10 mbsf, Hole M0061B = 2.40–7.89 mbsf, Hole M0061C = 2.44–8.74 mbsf

Unit II shows increasing magnetic susceptibility values downcore and a distinctive spike related to an iron sulfide clay subunit at 6.46–6.90 mcd. In the seismic profile, the lower limit corresponds to a very strong reflector, which could be a basin-wide erosional surface. This strong reflector could possibly be connected to a ~10 cm thick sandy bed observed between Units II and III (see “**Lithostratigraphy**”).

Seismic Unit III

Two-way traveltime: 0.140 ms

Lithology: dark greenish gray clayey silt with a varvic rhythmic lamination (lithostratigraphic Unit III)

Depths: Hole M0061A = 8.10–14.50 mbsf, Hole M0061B = 7.89–14.50 mbsf, Hole M0061C = 8.74–15.20 mbsf

Unit III shows increasing rhythmic variations in downcore magnetic susceptibility values. The lower boundary of seismic Unit III is characterized in the seismic profiles by closely spaced dark reflectors, possibly indicating gradual thickening of rhythmic laminae, and an increase in silt and sand content.

Seismic Unit IV

Two-way traveltime: 0.159 ms

Lithology: dark gray silty sand and fine sand with a few dispersed pebble-sized clasts (lithostratigraphic Unit IV)

Depths: Hole M0061A = 14.50–25.15 mbsf, Hole M0061B = 14.50–28.70 mbsf, Hole M0061C = 15.20–23.10 mbsf

Unit IV is characterized in the seismic images by an upper laminated part and a lower homogeneous part. However, the cores did not reveal this lamina-

tion/bedding, as the core liners were in many cases partly filled with water, so original sedimentary structures could not be verified.

References

- Andrén, T., Jørgensen, B.B., Cotterill, C., Green, S., Andrén, E., Ash, J., Bauersachs, T., Cragg, B., Fanget, A.-S., Fehr, A., Granoszewski, W., Groeneveld, J., Hardisty, D., Herrero-Bervera, E., Hyttinen, O., Jensen, J.B., Johnson, S., Kenzler, M., Kotilainen, A., Kotthoff, U., Marshall, I.P.G., Martin, E., Obrochta, S., Passchier, S., Quintana Krupinski, N., Riedinger, N., Slomp, C., Snowball, I., Stepanova, A., Strano, S., Torti, A., Warnock, J., Xiao, N., and Zhang, R., 2015a. Methods. *In* Andrén, T., Jørgensen, B.B., Cotterill, C., Green, S., and the Expedition 347 Scientists, *Proc. IODP*, 347: College Station, TX (Integrated Ocean Drilling Program). doi:10.2204/iodp.proc.347.102.2015
- Andrén, T., Jørgensen, B.B., Cotterill, C., Green, S., Andrén, E., Ash, J., Bauersachs, T., Cragg, B., Fanget, A.-S., Fehr, A., Granoszewski, W., Groeneveld, J., Hardisty, D., Herrero-Bervera, E., Hyttinen, O., Jensen, J.B., Johnson, S., Kenzler, M., Kotilainen, A., Kotthoff, U., Marshall, I.P.G., Martin, E., Obrochta, S., Passchier, S., Quintana Krupinski, N., Riedinger, N., Slomp, C., Snowball, I., Stepanova, A., Strano, S., Torti, A., Warnock, J., Xiao, N., and Zhang, R., 2015b. Site M0062. *In* Andrén, T., Jørgensen, B.B., Cotterill, C., Green, S., and the Expedition 347 Scientists, *Proc. IODP*, 347: College Station, TX (Integrated Ocean Drilling Program). doi:10.2204/iodp.proc.347.106.2015
- Frenzel, P., Keyser, D., and Viehberg, F.A., 2010. An illustrated key and (palaeo)ecological primer for postglacial to Recent Ostracoda (Crustacea) of the Baltic Sea. *Boreas*, 39(3):567–575. doi:10.1111/j.1502-3885.2009.00135.x
- Hajdu, S., Larsson, U., and Skärlund, K., 1997. Växtplankton. *In* Elmgren, R., and Larsson, U. (Eds.), *Himmerfjärden: förändringar i ett näringsbelastat kustekosystem i Östersjön* (Rapport 4565): Stockholm (Naturvårdsverket-förlag), 63–79. (in Swedish, with abstract in English)
- Hasle, G.R., and Syvertsen, E.E., 1990. Arctic diatoms in the Oslofjord and the Baltic Sea—a bio- and palaeogeographic problem. *In* Simmola, H. (Ed.), *Proceedings of the 10th International Diatom Symposium*: Koenigstein, Germany (Koeltz Scientific Books), 285–300.
- Hedenström, A., and Risberg, J., 1999. Early Holocene shore-displacement in southern central Sweden as recorded in elevated isolated basins. *Boreas*, 28(4):490–504. doi:10.1111/j.1502-3885.1999.tb00236.x
- Huntley, B., and Birks, H.J.B., 1983. *An Atlas of Past and Present Pollen Maps for Europe: 0–13,000 Years Ago*: Cambridge, U.K. (Cambridge Univ. Press).
- Lutze, G.F., 1965. Zur foraminiferen-fauna der ostsee (The distribution of foraminifera in the Baltic Sea). *Meyniana*, 15:75–142.
- Mertens, K.N., Ribeiro, S., Bouimetarhan, I., Caner, H., Nebout, N.C., Dale, B., De Vernal, A., Ellegaard, M., Filipova, M., Godhe, A., Goubert, E., Grøsfjeld, K., Holz-

- warth, U., Kotthoff, U., Leroy, S.A.G., Londeix, L., Marret, F., Matsuoka, K., Mudie, P.J., Naudts, L., Peña-Manjarrez, J.L., Persson, A., Popescu, S.-M., Pospelova, V., Sangiorgi, F., van der Meer, M.T.J., Vink, A., Zonneveld, K.A.F., Vercauteren, D., Vlassenbroeck, J., and Louwe, S., 2009. Process length variation in cysts of a dinoflagellate, *Lingulodinium machaerophorum*, in surface sediments: investigating its potential as salinity proxy. *Mar. Micropaleontol.*, 70(1–2):54–69. doi:10.1016/j.marmicro.2008.10.004
- Nehring, S., 1994. *Dinoflagellaten-Dauercysten in deutschen Küstengewässern: Vorkommen, Verbreitung und Bedeutung als Rekrutierungspotential*. Ber. Inst. Meereskd. Christian-Albrechts-Univ., Kiel, 259.
- Rottgardt, D., 1952. Mikropaläontologische wichtige Bestandteile rezenter brakischer Sedimente an den Küsten Schleswig-Holsteins. *Meyniana* 1:169–228.
- Roussel, E.G., Cambon Bonavita, M.-A., Querellou, J., Cragg, B.A., Webster, G., Prieur, D., and Parkes, J.R., 2008. Extending the sub-sea-floor biosphere. *Science*, 320(5879):1046. doi:10.1126/science.1154545
- Samuelsson, M., 1996. Interannual salinity variations in the Baltic Sea during the period 1954–1990. *Cont. Shelf Res.*, 16(11):1463–1477. doi:10.1016/0278-4343(95)00082-8
- Segerström, U., and von Stedingk, H., 2003. Early Holocene spruce, *Picea abies* (L.) Karst., in west central Sweden as revealed by pollen analysis. *Holocene*, 13(6):897–906. doi:10.1191/0959683603hl672rp
- Snoeijs, P., Vilbaste, S., Potapova, M., Kasperoviciene, J., and Balashova, J. (Eds.), 1993–1998. *Intercalibration and Distribution of Diatom Species in the Baltic Sea* (Vol. 1–5): Uppsala, Sweden (Opulus Press).
- Snowball, I., Zillén, L., Ojala, A., Saarinen, T., and Sandgren, P., 2007. FENNOSTACK and FENNORPIS: varve dated Holocene palaeomagnetic secular variation and relative palaeointensity stacks for Fennoscandia. *Earth Planet. Sc. Lett.*, 255(1–2):106–116. doi:10.1016/j.epsl.2006.12.009
- Snowball, I.F., 1997. Gyroremanent magnetization and the magnetic properties of greigite-bearing clays in southern Sweden. *Geophys. J. Int.*, 129(3):624–636. doi:10.1111/j.1365-246X.1997.tb04498.x
- Weckström, K., and Juggins, S., 2006. Coastal diatom–environment relationships from the Gulf of Finland, Baltic Sea. *J. Phycol.*, 42(1):21–35. doi:10.1111/j.1529-8817.2006.00166.x
- Widerlund, A., and Andersson, P.S., 2011. Late Holocene freshening of the Baltic Sea derived from high-resolution strontium isotope analyses of mollusk shells. *Geology*, 39(2):187–190. doi:10.1130/G31524.1

Publication: 20 February 2015
MS 347-105

Figure F1. Graphic lithology log summary, Hole M0061A and base of Hole M0061B.

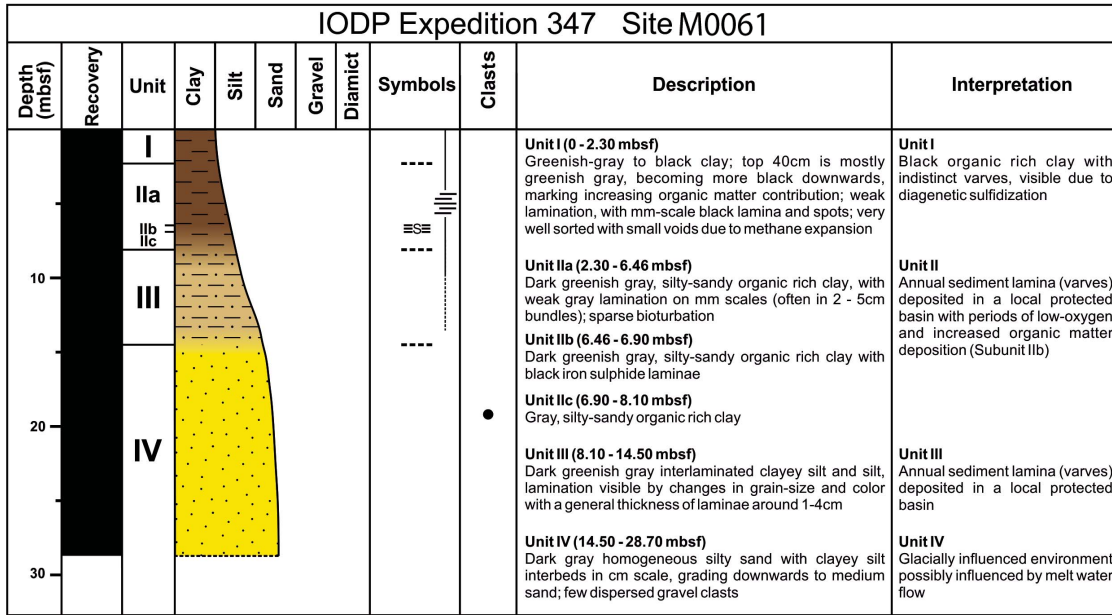


Figure F2. Black laminated horizon (Subunit IIa) that represents increased iron sulfide diagenetic processes (interval 347-M0061A-3H-2, 2–69 cm).

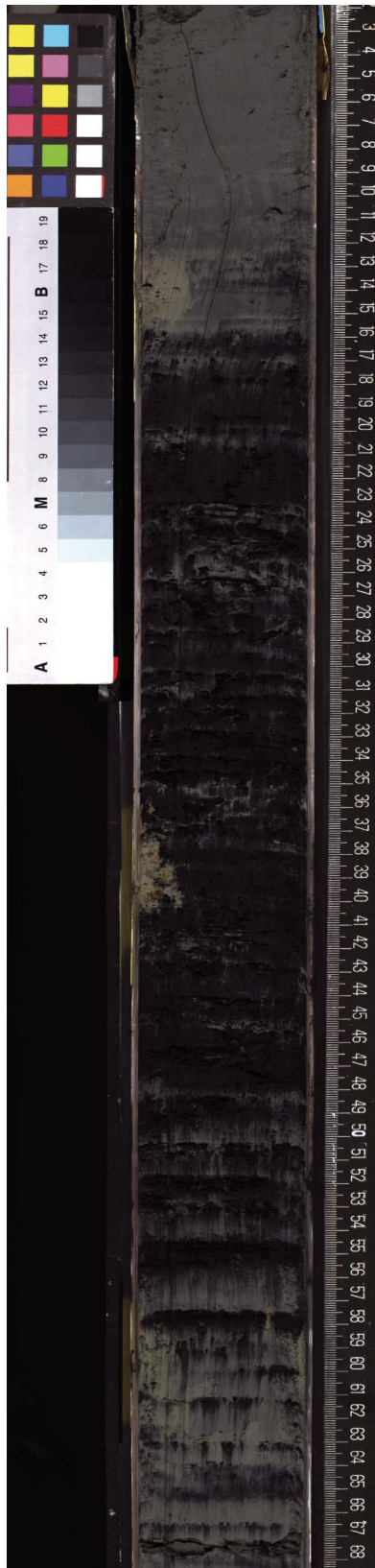


Figure F3. Analyzed levels of siliceous microfossils and the proportion of diatom taxa showing different salinity affinities, Site M0061. The total number of diatom taxa recorded is plotted, as well as the number of taxa associated with planktonic, periphytic, and sea ice related taxa. Red dots indicate presence of sea ice related taxa and other siliceous microfossils recorded in the cores. This graph must be interpreted with caution because it is based only on qualitative analyses. Each species was counted only present or absent, so a species represented by a single valve carries as much weight as a species dominating the assemblage.

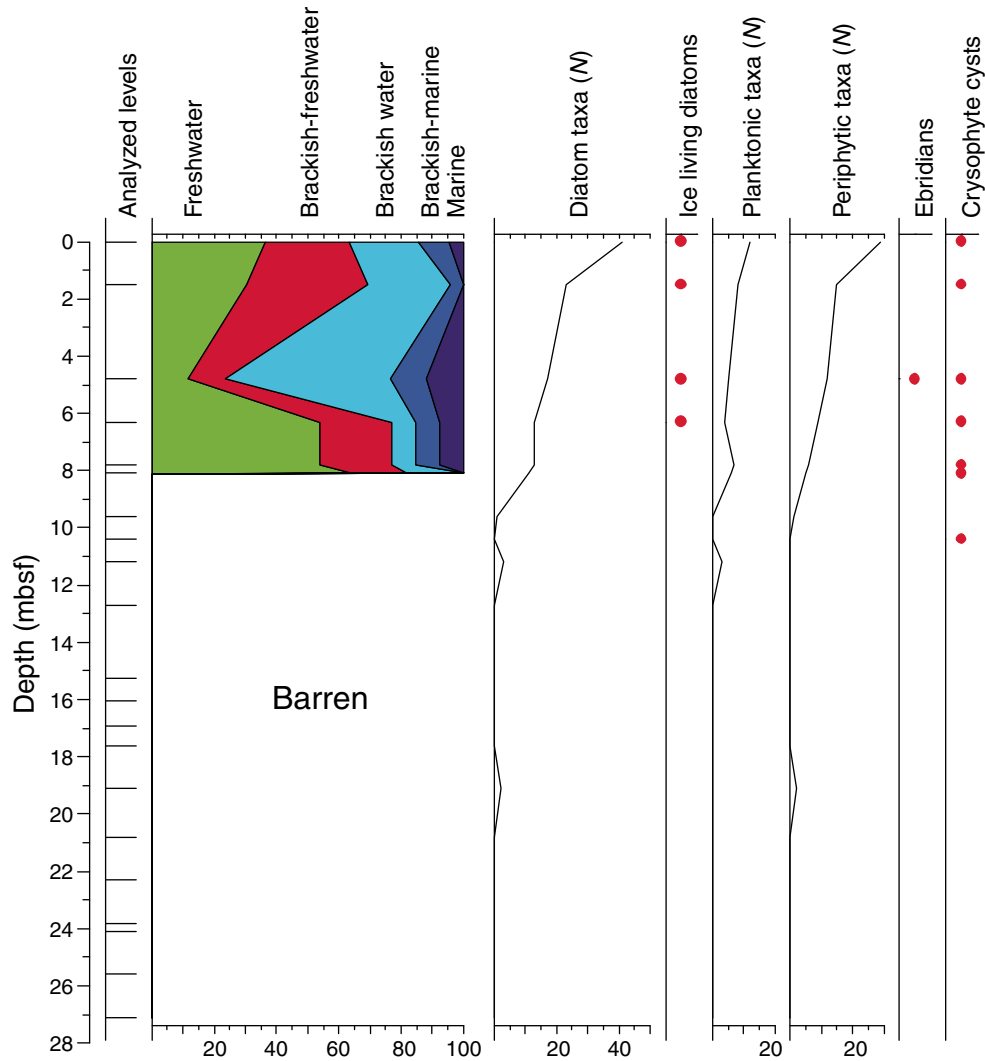


Figure F4. Analyzed levels of siliceous microfossils and the proportion of diatom taxa showing different salinity affinities, Hole M0061B. The total number of diatom taxa recorded is plotted, as well as the number of taxa associated to planktonic, periphytic, and sea ice related taxa. Red dots indicate presence of sea ice related taxa and other siliceous microfossils recorded in the cores. This graph must be interpreted with caution because it is based only on qualitative analyses. Each species was counted only present or absent, so a species represented by a single valve carries as much weight as a species dominating the assemblage.

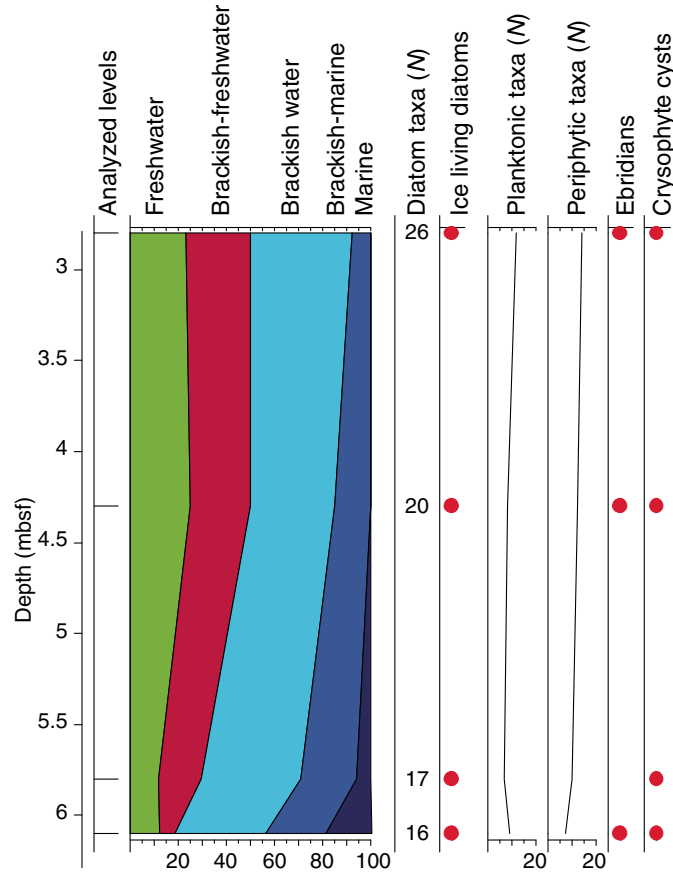


Figure F5. Abundance of benthic foraminifers based on the abundance classification defined in the “**Methods**” chapter (Andrén et al., 2015a), Site M0061. A running average over three samples is plotted onto single data points. Increasing shading indicates abundances sufficient for faunal and/or geochemical analyses.

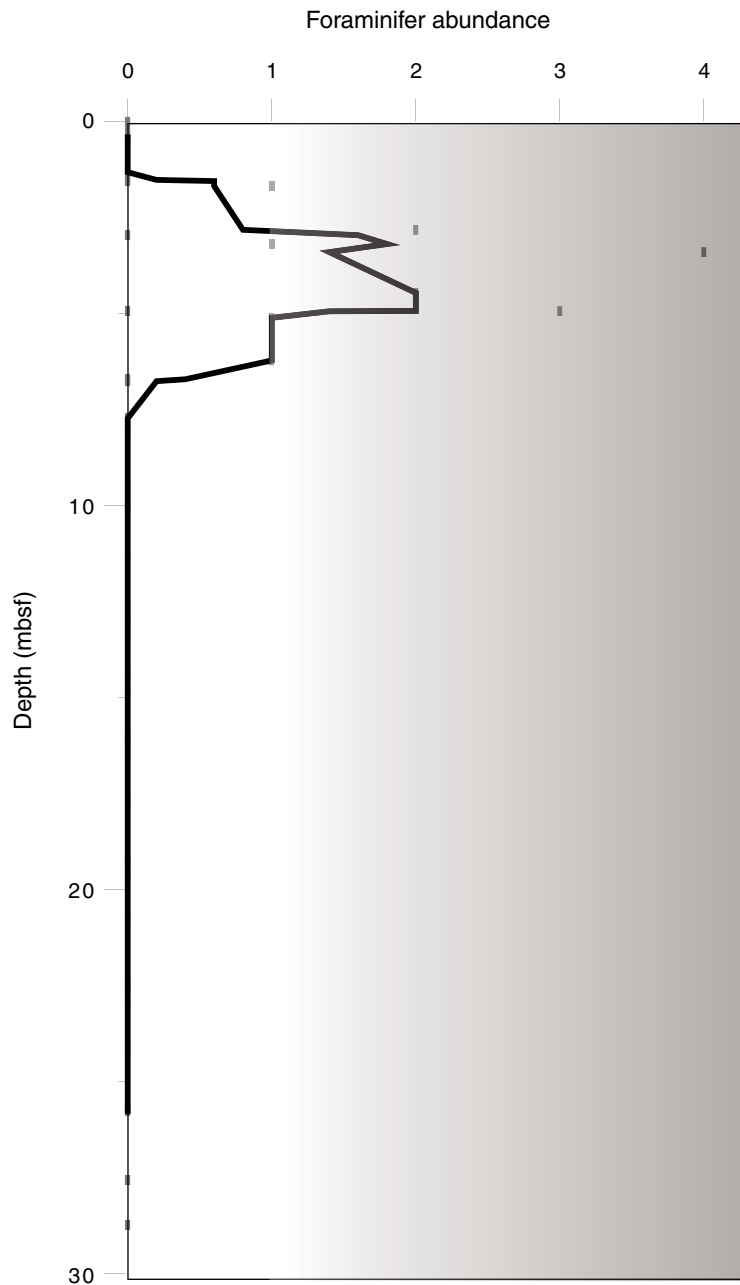


Figure F6. Ostracod abundance, Site M0061. Abundance is shown per sediment volume.

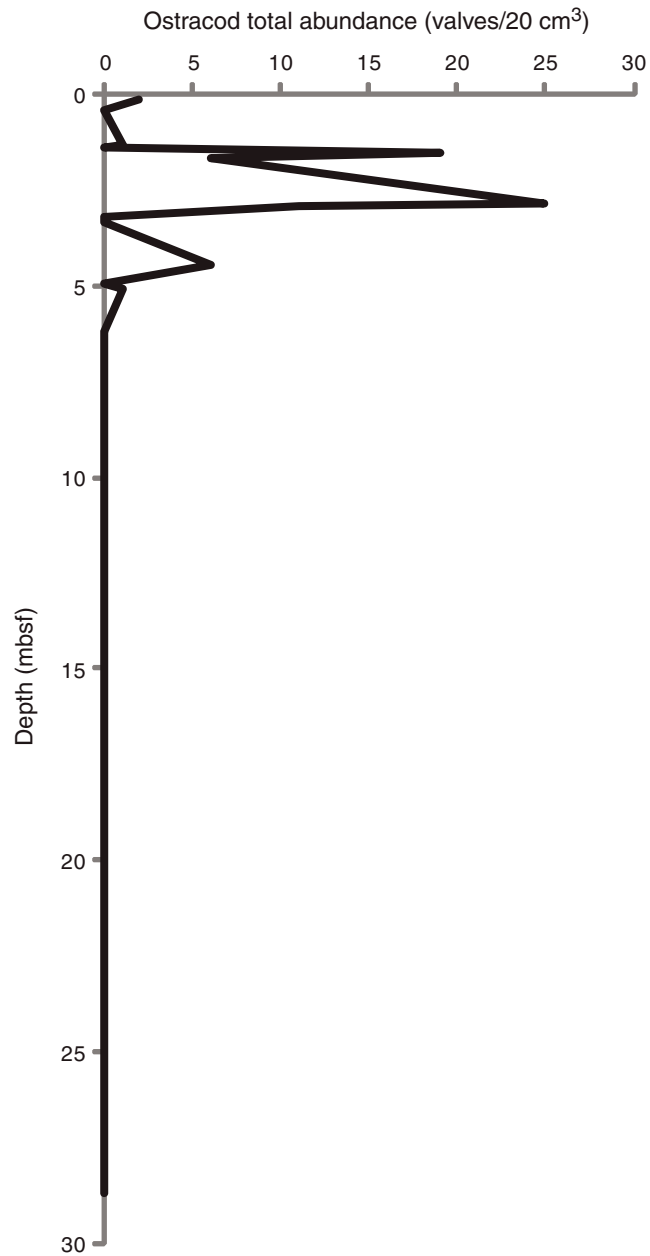




Figure F7. Pollen diagram with bisaccate pollen included in the reference sum, Hole M0061B. For all samples, between 150 and 310 grains have been counted.

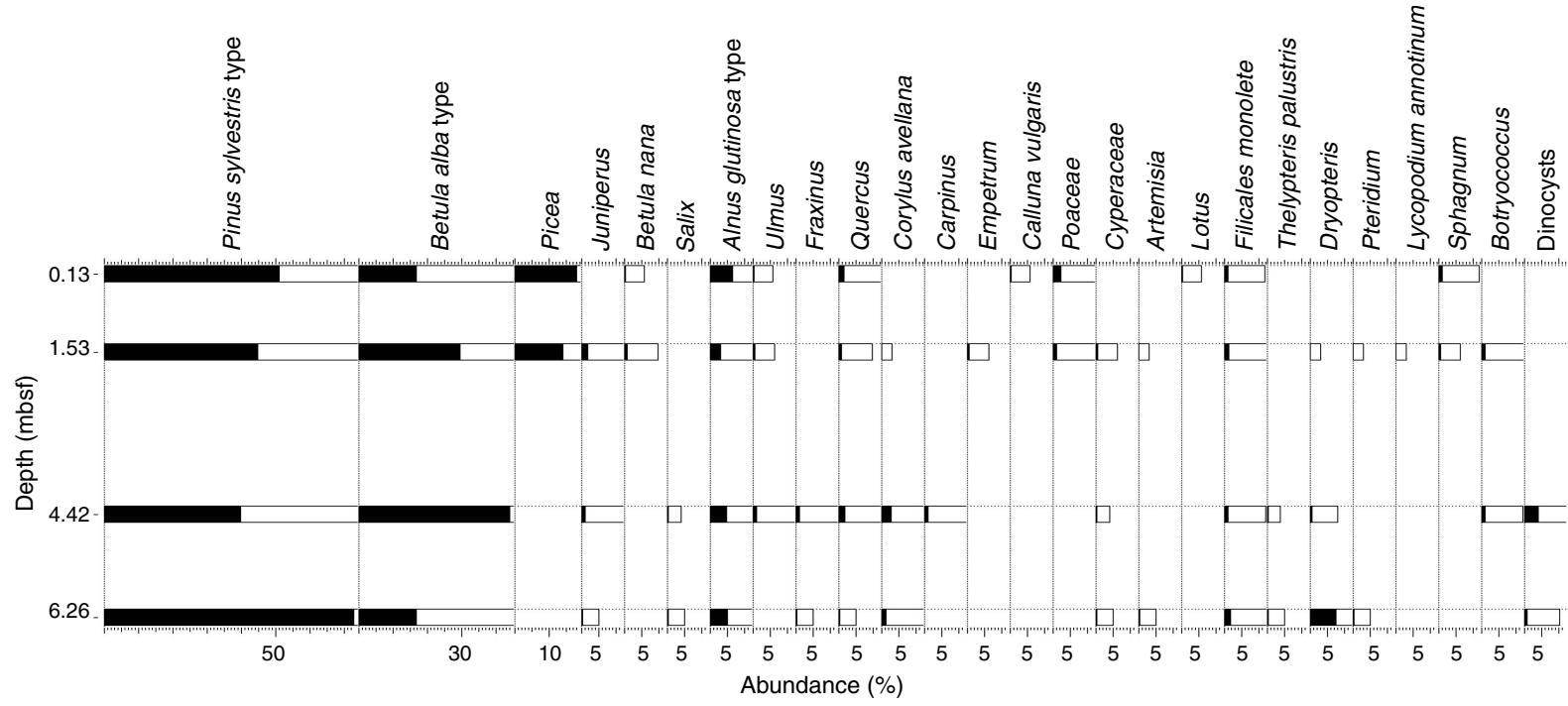


Figure F8. Simplified pollen diagram with main pollen types, further palynomorph data, and occurrences of *Radiosperma corbiferum*, Hole M0061B.

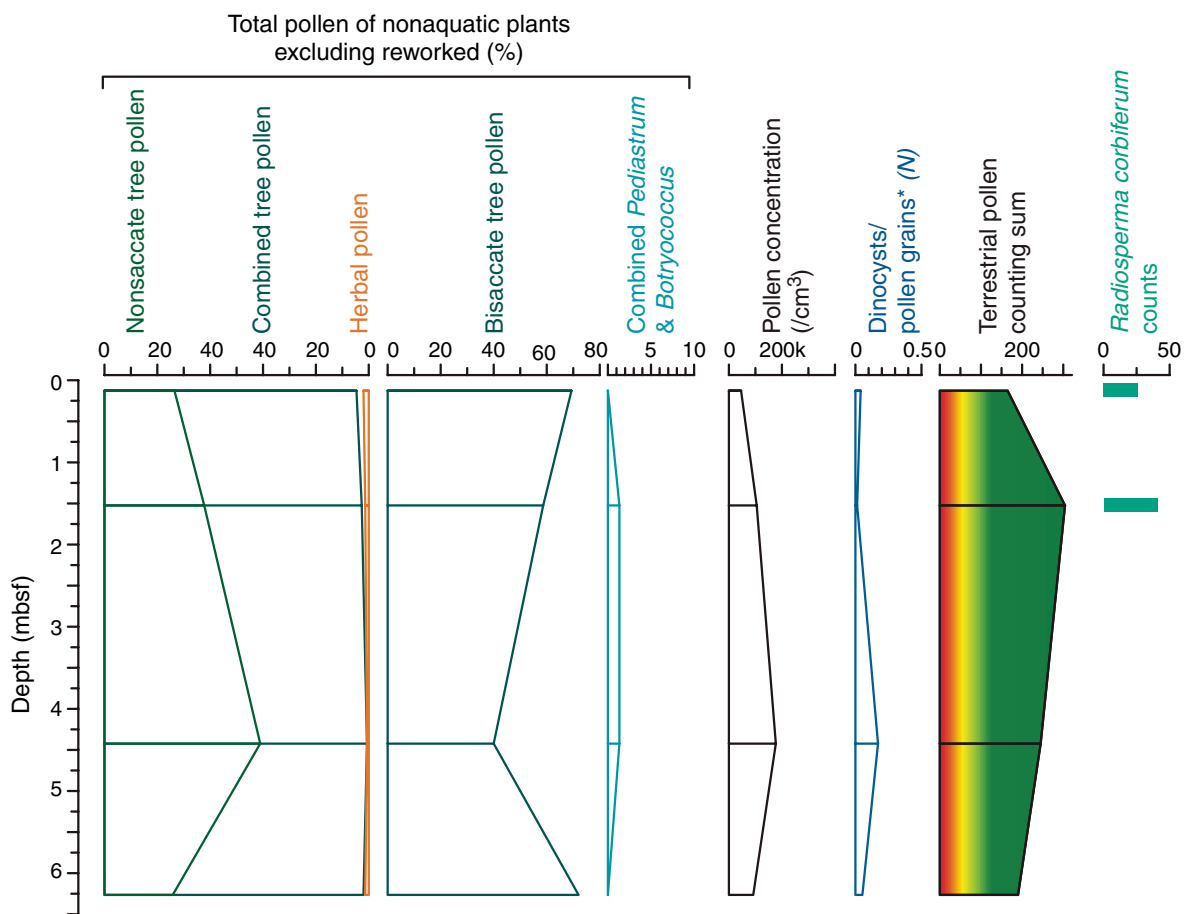




Figure F9. Concentrations of (A) chloride, (B) salinity, (C) chloride-based salinity by refractometer, and (D) alkalinity in interstitial water samples, Site M0061.

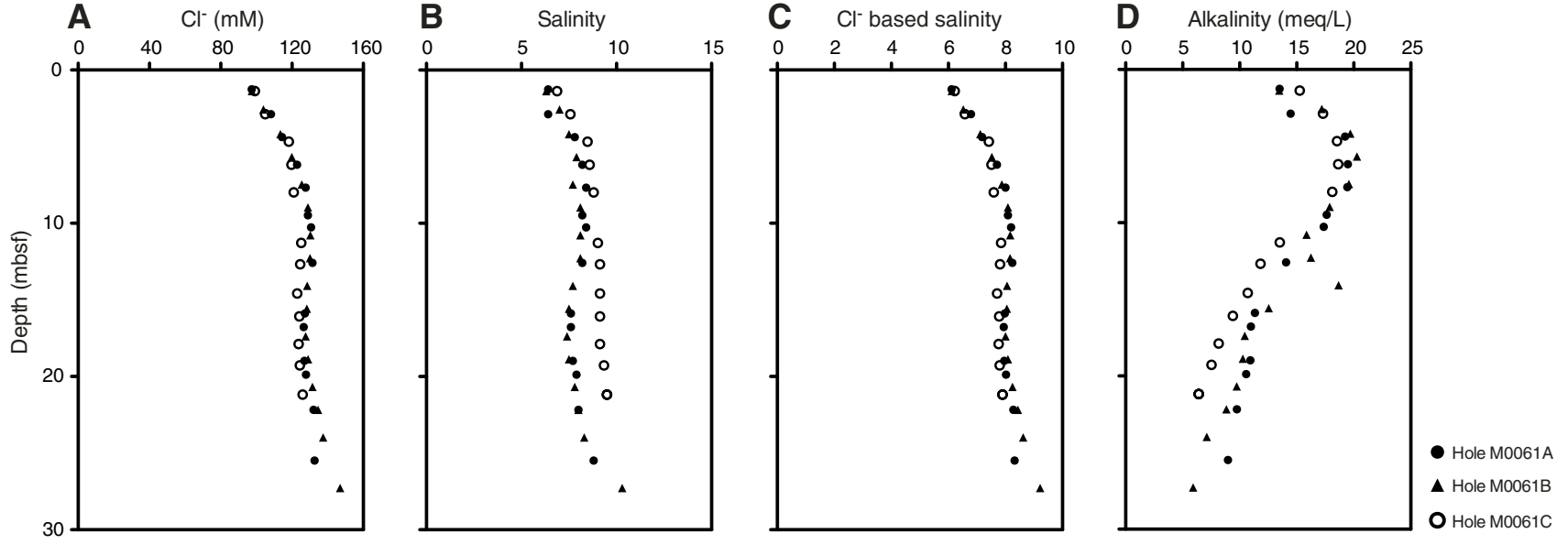




Figure F10. Concentrations of (A) sulfate, (B) sulfide, (C) ammonium, (D) phosphate, (E) iron, (F) manganese, and (G) pH from interstitial water samples, Site M0061.

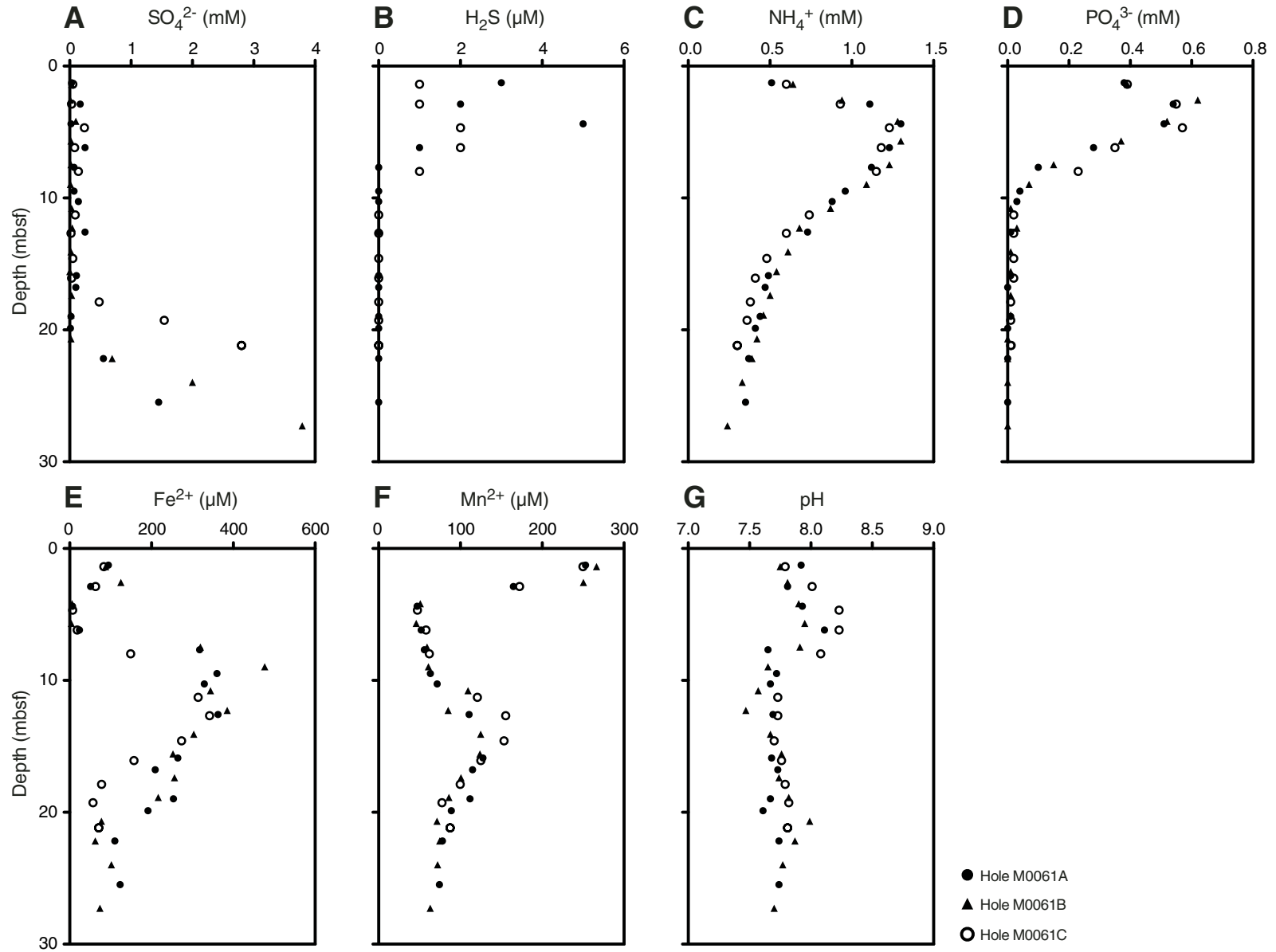




Figure F11. Concentrations and ratios of (A) bromide, (B) bromide/chloride, (C) boron, and (D) boron/chloride from interstitial water samples, Site M0061. Dashed lines = seawater ratio.

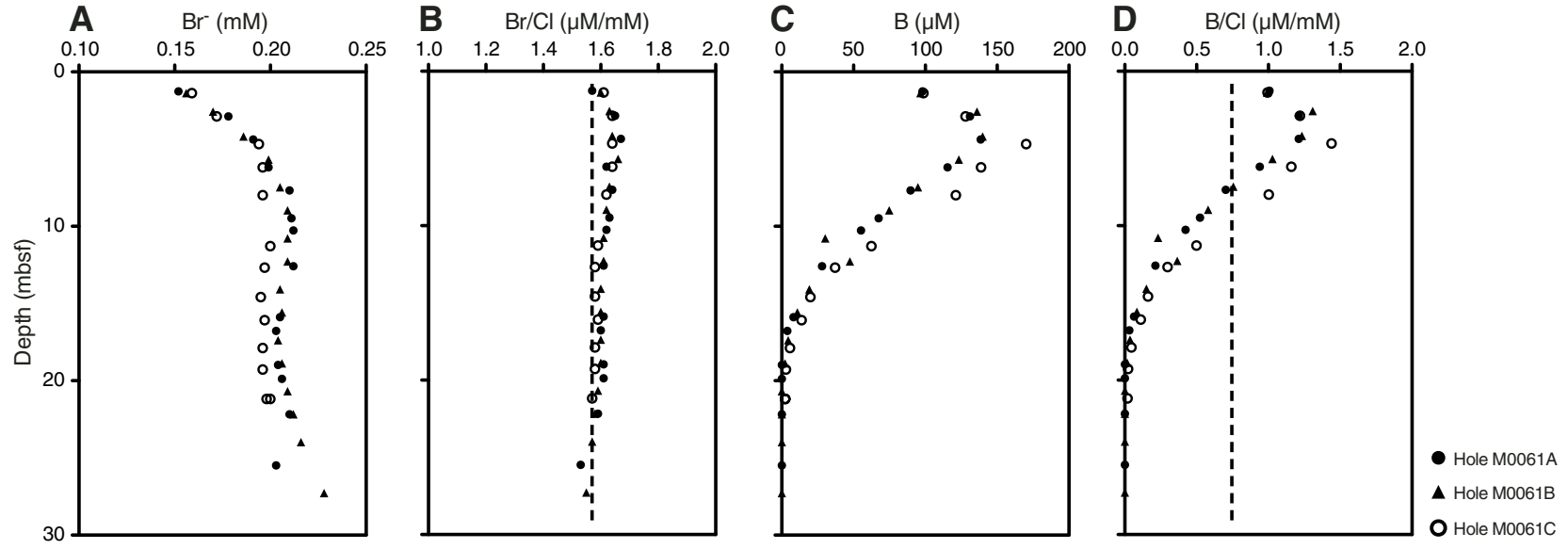




Figure F12. Concentrations and ratios of (A) sodium, (B) potassium, (C) magnesium, (D) calcium, (E) sodium/chloride, (F) potassium/chloride, (G) magnesium/chloride, and (H) calcium/chloride in interstitial water samples, Site M0061. Dashed lines = seawater ratio.

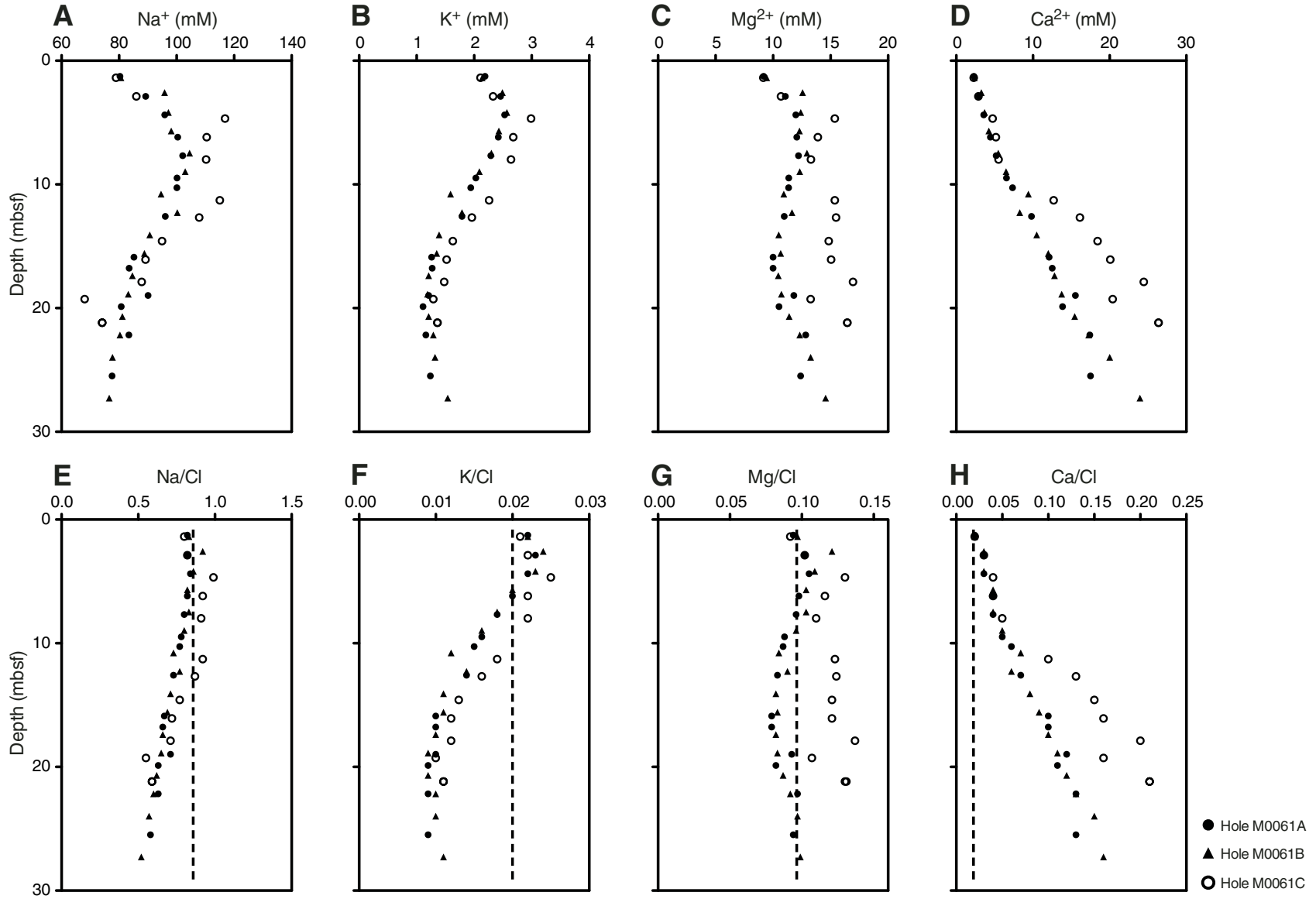




Figure F13. Concentrations of (A) strontium, (B) lithium, (C) dissolved silica, and (D) barium from interstitial water samples, Site M0061.

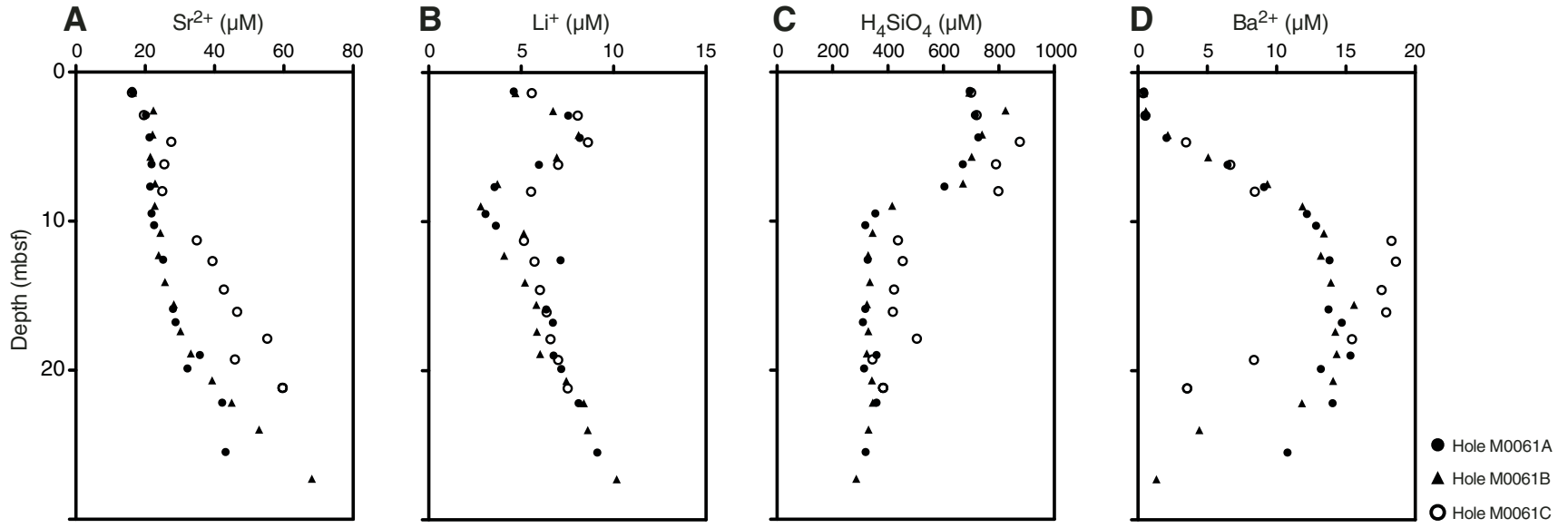




Figure F14. Solid phase concentrations of (A) total carbon (TC), (B) total organic carbon (TOC), (C) total inorganic carbon (TIC), and (D) total sulfur (TS), Site M0061.

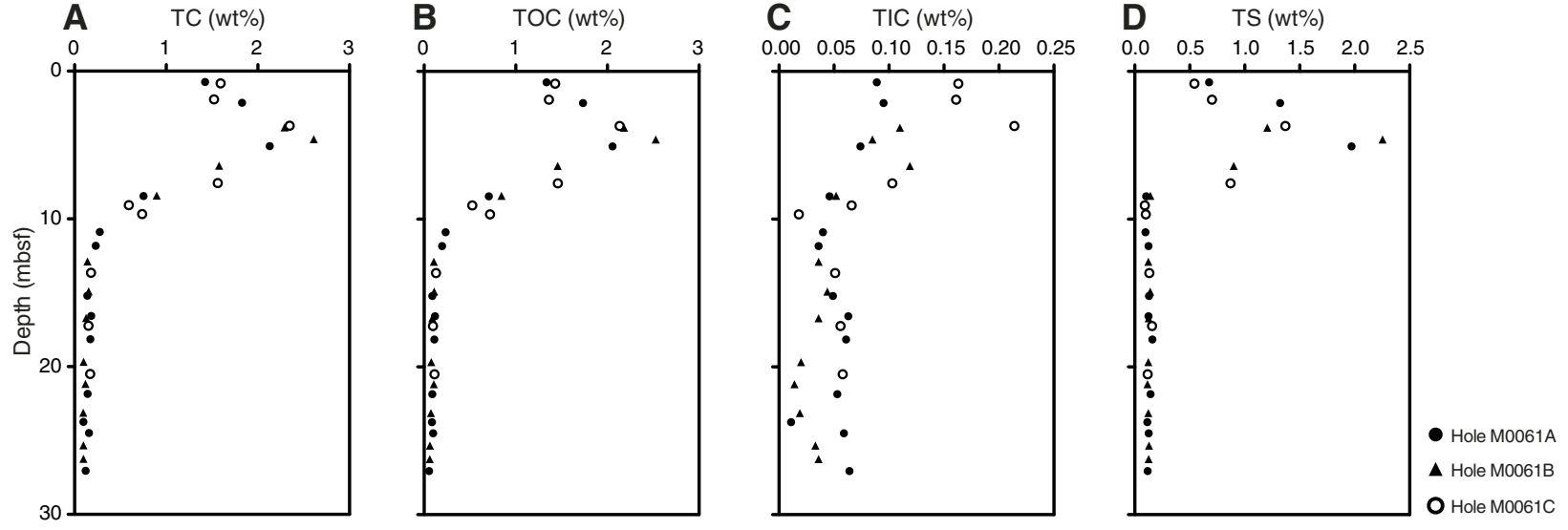


Figure F15. Magnetic susceptibility (MS) (10^{-5} SI), natural gamma radiation (NGR) (cps), noncontact resistivity (NCR) (Ωm), P -wave velocity (m/s), and b^* , Hole M0061B.

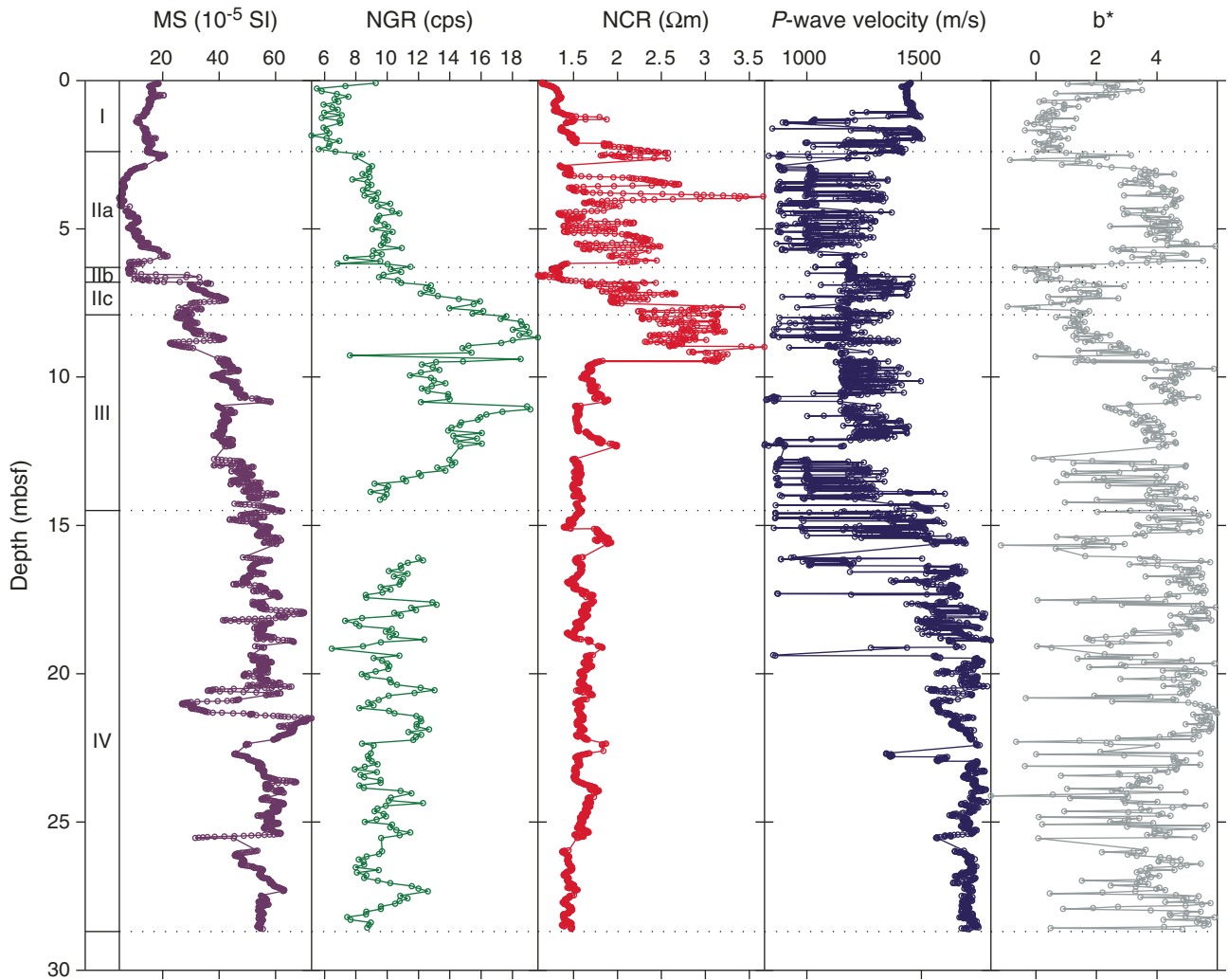


Figure F16. Gamma density (g/cm^3) and discrete bulk density (g/cm^3) measurements derived from pycnometer moisture and density analyses, Hole M0061B.

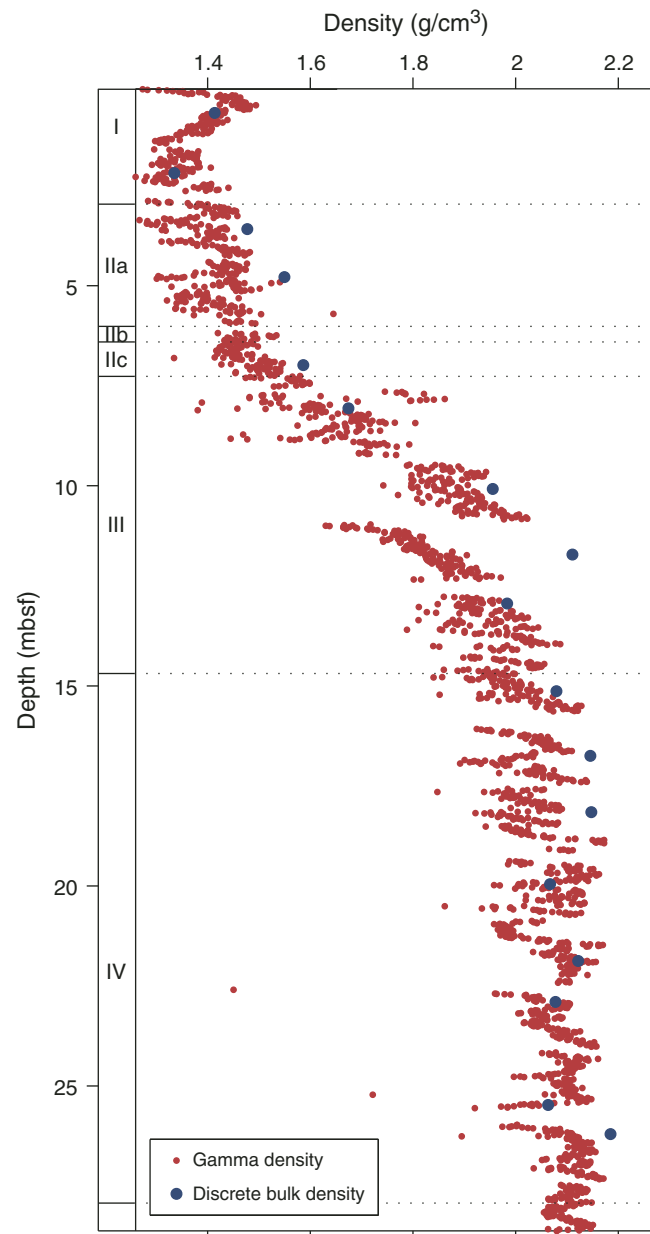


Figure F17. Gamma density (g/cm^3) and discrete bulk density (g/cm^3) measurements are highly correlated in Hole M0061B.

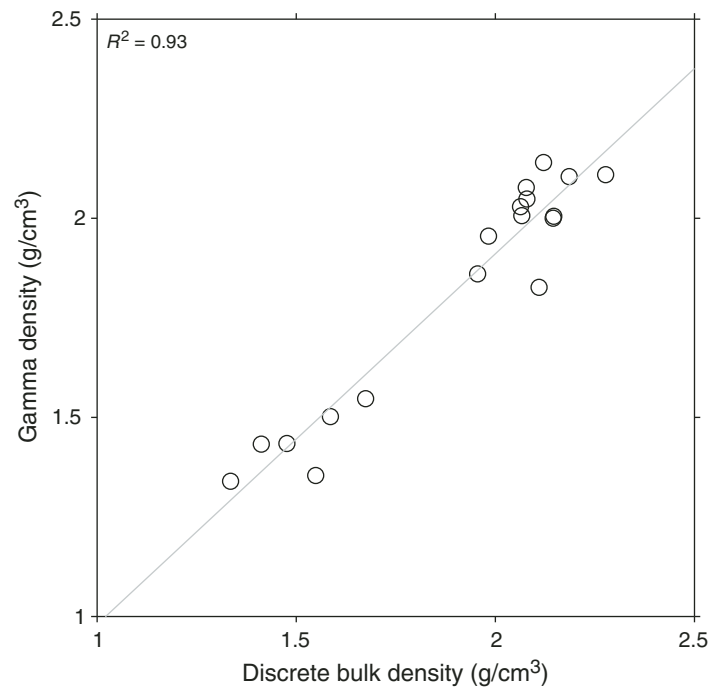




Figure F18. Plots and biplots of magnetic susceptibility (χ), natural remanent magnetization (NRM) intensity, and NRM inclination of discrete paleomagnetic samples, Hole M0061A. Dashed line = geocentric axial dipole (GAD) prediction of inclination for the site latitude. AF = alternating field.

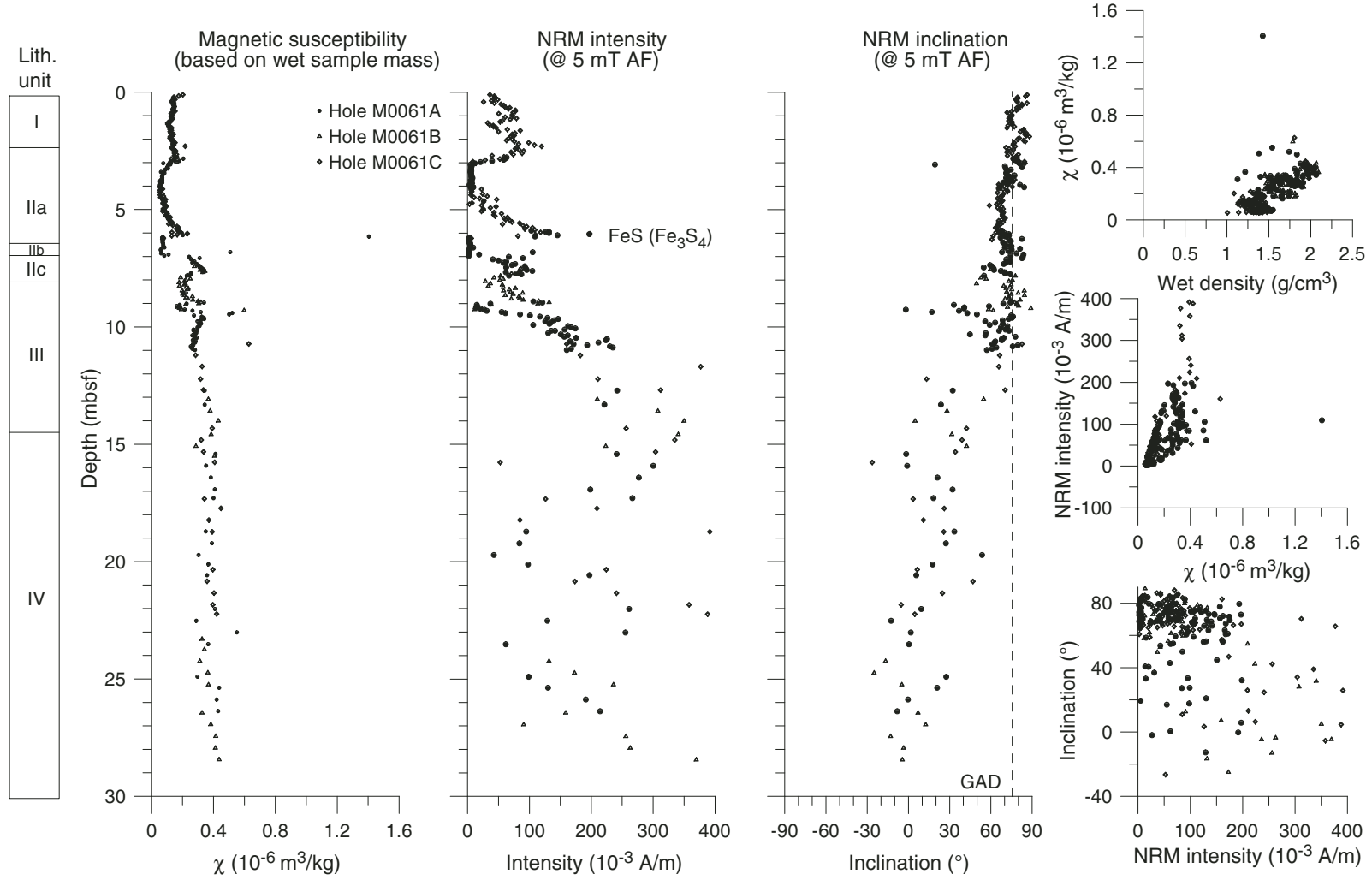


Figure F19. Plots of natural remanent magnetization after alternating field (AF) demagnetization to 80 mT. **A.** Sample 347-M0061A-3H-1, 89 cm; 5.89 mcd. **B.** Sample 347-M0061A-4H-1, 138 cm; 9.81 mcd. **C.** Sample 347-M0061A-9H-2, 120 cm; 22.01 mcd. Category 2 and 3 vectors trend toward the origin and display high magnetic stability, whereas Category 1 vectors contain a low-stability component. The vector veers into a plane perpendicular to the last demagnetization axis, which is a sign of gyroremanent magnetization acquisition. Open squares = vertical, solid squares = horizontal.

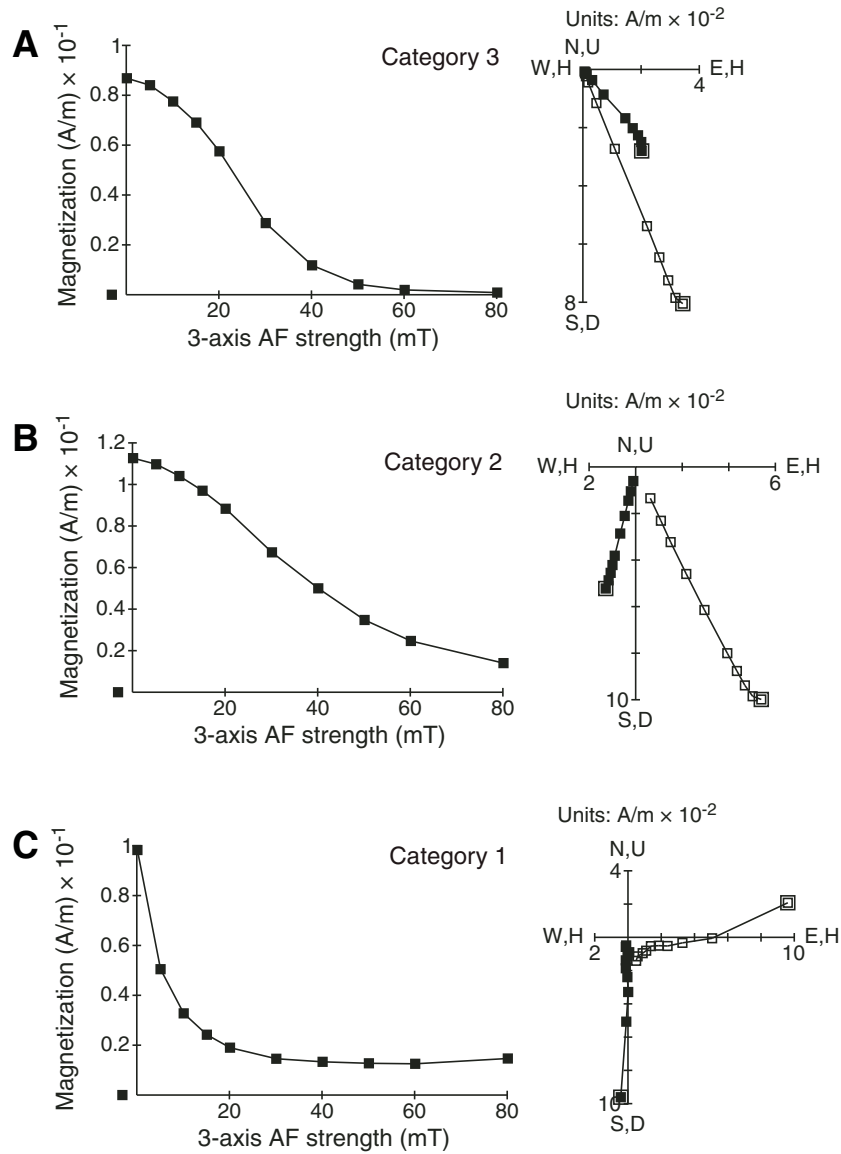


Figure F20. Plot of microbial cell abundance (red diamonds), Hole M0061K. Solid black line = global regression line of prokaryote cell numbers with depth, dashed lines = upper and lower 95% prediction limits for regression line (Roussel et al., 2008).

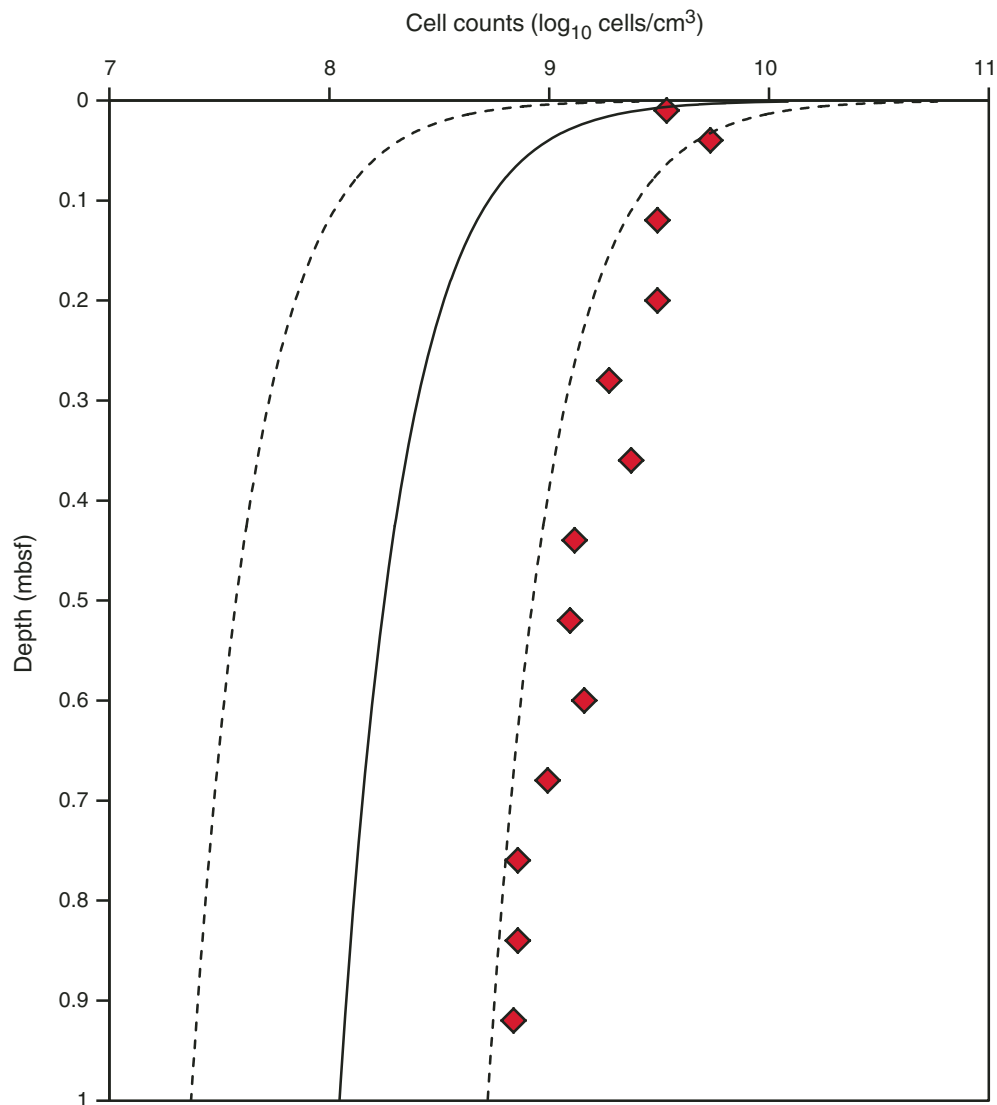


Figure F21. Plot of spliced magnetic susceptibility data, Holes M0061A–M0061C. Letters and numbers at the top refer to holes and core runs, respectively, used in the splice.

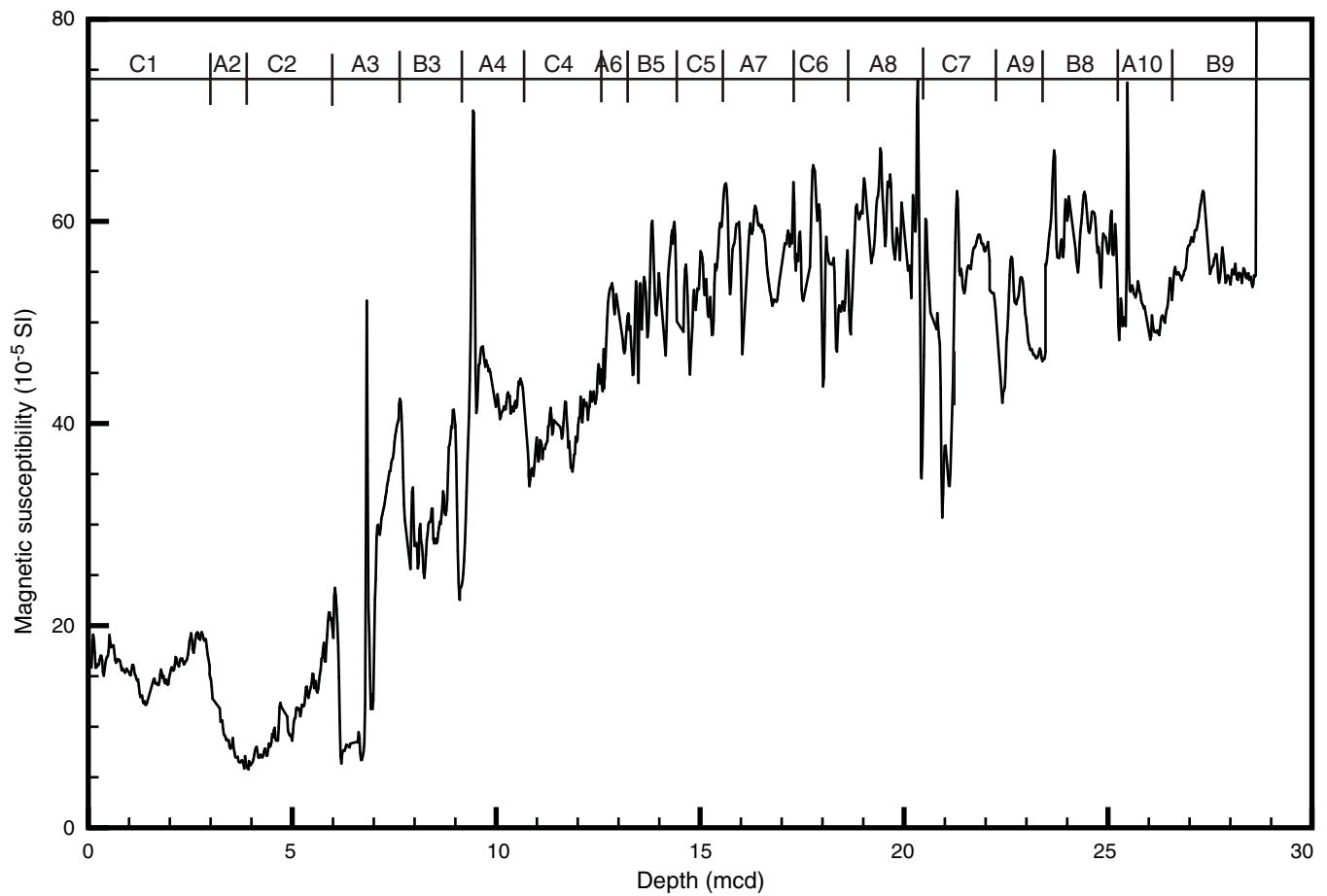


Figure F22. Correlation of the seismic profile with lithostratigraphic units (I–IV) and multisensor core logger magnetic susceptibility data (Hole M0061A), Site M0061.

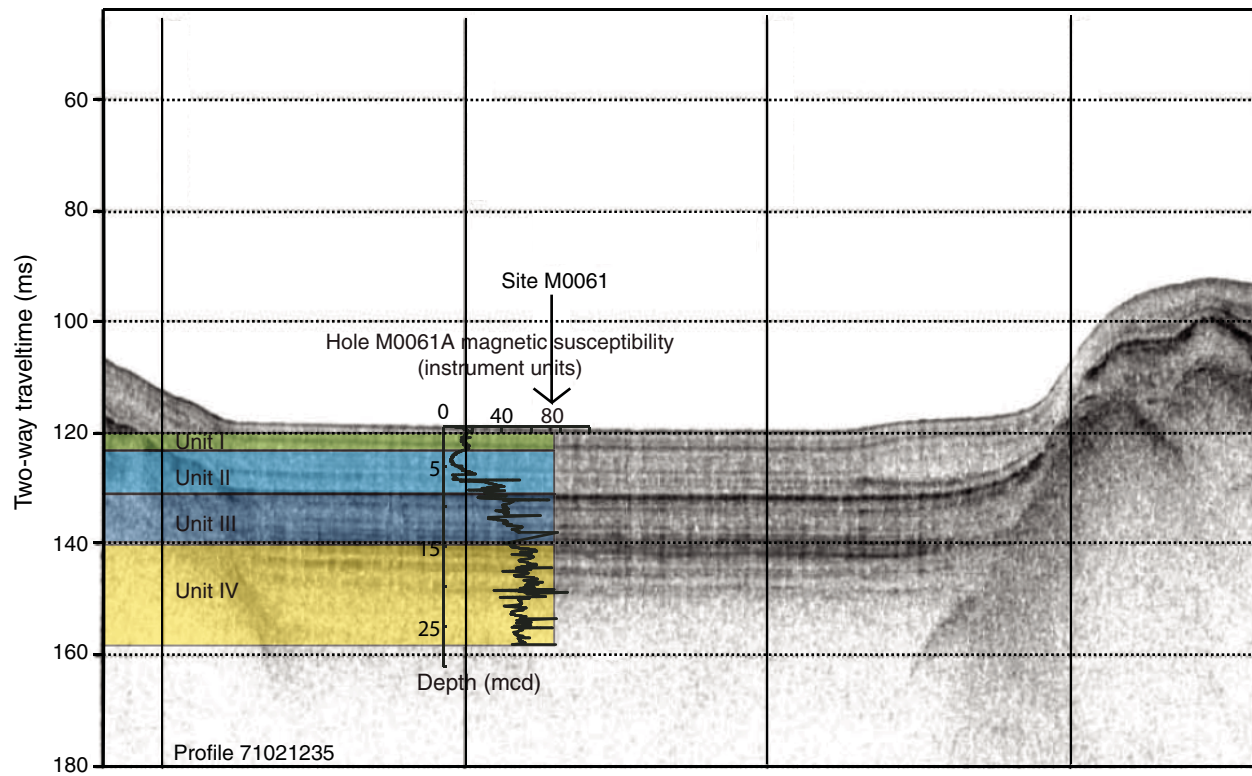




Table T1. Operations, Site M0061.

Core	Coring method	Date (2013)	Time (UTC)	Depth (mbsf)		Recovered (m)	Recovery (%)	Mud type	Comments
				Top	Bottom				
347-M0061A-									
		4 Oct	1230						Seabed template not lowered, piston fired in water at 0.5 m above the estimated mudline to capture sediment/water interface; on recovery, water depth reassessed and string lowered to calculated mudline
1H	PCS	4 Oct	1335	0.00	1.50	1.53	102	Seawater	Drilled out 3.3 m from last sample, added pipe, and lowered seabed template to seabed
2H	PCS	4 Oct	1355	1.50	4.80	3.44	104.24	Seawater	65 bar; good fire sequence, good recovery
3H	PCS	4 Oct	1520	4.80	8.10	3.28	99.39	Seawater	
4H	PCS	4 Oct	1555	8.10	11.20	3.18	102.58	Seawater	Barrel stuck; eventually freed after hammering with overshot and pumping water
5H	PCS	4 Oct	1630	11.20	11.20	0.00	0	Seawater	Stopped to fix deck lights, which failed to come back on following a ship power failure
6H	PCS	4 Oct	1718	11.20	14.50	2.13	64.55	Seawater	Piston fired at 60 bar
7H	PCS	4 Oct	1834	14.50	17.60	3.18	102.58	Seawater	Pressurized up to 220 bar without any apparent firing point; on release of pressure and recovery of the corer, we had collected 3.3 m of very fine to fine sand
8H	PCS	4 Oct	1935	17.60	20.80	3.17	99.06	Seawater	Prepared drill floor to lift template; lifted template and positioned large transponder; returned template to seabed and replaced mouseholes
9H	PCS	4 Oct	2030	20.80	24.10	3.30	100	Guar	Washed down to 24.1 mbsf and ran PCS
10H	PCS	4 Oct	2054	24.10	25.10	3.15	315	Guar	Pressure reached 135 bar; sample probably sucked in
11S	HS	4 Oct	2220	25.10	25.20	0.10	100	Guar	Hammer sample when no progress made while washing down from 24.1 mbsf; recovered rock—looks like bedrock rather than clast or pebble
		4 Oct	2300						Pulled string
347-M0061B-									
		4 Oct	2340						Started lowering drill string
1H	PCS	5 Oct	0000	0.00	2.80	2.83	101.07	Seawater	Fired piston from ~0.5 m above seabed
2H	PCS	5 Oct	0025	2.80	6.10	3.43	103.94	Seawater	
3H	PCS	5 Oct	0113	6.10	9.40	3.44	104.24	Seawater	10 bar then zero
4H	PCS	5 Oct	0143	9.40	12.70	3.15	95.45	Seawater	Not a clean fire; 50 bar, dropped then went up to 125 bar before dropping away quickly; bottom of core run was more silty if not sandy; changed to Guar mud while drilling down
5H	PCS	5 Oct	0211	12.70	16.00	3.17	96.06	Guar	50 bar, then up to 80 bar, then rising to 100 bar before dropping and then rising to 125 bar and dropping all the way; possible sand/silt layers; still very soft at the bottom
6H	PCS	5 Oct	0245	16.00	19.30	3.30	100	Guar	Same firing pattern as before but less pressure after firing
7H	PCS	5 Oct	0320	19.30	22.60	3.21	97.27	Guar	50 bar, then up to 80 then 100 then 130 bar before dropping to zero; still sand indications
8H	PCS	5 Oct	0450	22.60	25.90	3.09	93.64	Guar	Fired as normal but pressure did not drop fully and then went up over 125 bar until the pipe was lifted
		5 Oct	0506						Tool stuck in the hole, hammer overshot but no release; ran overshot release and tried to free by pumping; recovered on the second attempt
9H	PCS	5 Oct	0545	25.90	28.70	2.83	101.07	Guar	Fired: other than slight pressure flicker, firing point was not discernible and continued upward, stopped by the driller at 125 bar; did not release pressure until rooster box was lifted; pumped before attempting recovery
		5 Oct	0604						Unable to release corer despite hammering; released overshot to allow more pumping; eventually successful in recovering corer after pumping and hammering with the overshot
		5 Oct	0645						Tripped pipe to allow bump over for Hole M0061B
347-M0061C-									
		5 Oct	0700						
1H	PCS	5 Oct	0725	0.00	3.30	3.41	103.33	Seawater	50 bar, right down to zero
2H	PCS	5 Oct	0805	3.30	6.60	3.42	103.64	Seawater	Fired normally
3H	PCS	5 Oct	0850	6.60	9.90	3.44	104.24	Seawater	Fired normally
4H	PCS	5 Oct	0915	9.90	13.20	3.14	95.15	Seawater	Fired, pressure up then down to zero
5H	PCS	5 Oct	1035	13.20	16.50	3.37	102.12	Seawater	50 bar, down to zero
6H	PCS	5 Oct	1110	16.50	19.80	3.22	97.58	Seawater	60 bar, down to zero
7H	PCS	5 Oct	1145	19.80	23.10	3.17	96.06	Seawater	110 bar, had to release pressure at pump
		5 Oct	1220						Tripped pipe
									Completed and awaiting pilot for transit to Site M0062

HS = hammer sampler, PCS = piston coring system.

Table T2. Diatoms, Hole M0061A. (Continued on next page.)

Affinity	Life form	Diatoms	Core, section, interval (cm):																						
			1H-1	2H-1	3H-1	3H-2	3H-CC	4H-1	4H-2	4H-3	6H-1	6H-2	7H-1, 77	7H-2, 2	7H-3, 2	8H-1	8H-2	9H-1	9H-2	9H-3	10H-1	10H-2	10H-3		
B	Episammic	<i>Achnanthes leonardii</i>	x																						
BF	Pelagic	<i>Achnanthes lemmermannii</i>				x																			
BF	Pelagic	<i>Actinocyclus octonarius</i> var. <i>tenellus</i>	x																						
BF	Epipellic	<i>Aneumastus minor</i>	x																						
F	Epipellic	<i>Aneumastus tusculus</i>	x																						
F		<i>Aulacoseira alpigena</i> (Grunow) Krammer		x				x		x						x									
F		<i>Aulacoseira ambigua</i>	x																						
F		<i>Aulacoseira granulata</i>	x																						
F		<i>Aulacoseira islandica</i>																							
F	Pelagic	<i>Aulacoseira islandica</i>																							
M/B	Pelagic	<i>Chaetoceros</i> resting spores spp.	x	x	x	x																			
M/B	Pelagic	<i>Chaetoceros</i> spp. vegetative cells																							
F	Epipsammic	<i>Cocconeis disculus</i>					x																		
BF	Epiphyte	<i>Cocconeis pediculus</i> Ehrenberg	x	x				x		x															
B	Pelagic	<i>Cocconeis scutellum</i>		x	x																				
BF	Pelagic	<i>Ctenophora pulchella</i> (Ralfs ex Kützing) Williams and Round		x																					
F	Pelagic	<i>Cyclotella atomus</i> Hustedt					x		x																
B	Pelagic and epilithic	<i>Cyclotella choctawhatcheeana</i>	x			x																			
BF	Pelagic	<i>Cyclotella meneghiniana</i>	x																						
F	Littoral?	<i>Cyclotella ocellata</i>	x																						
F	Pelagic	<i>Cyclotella radiosa</i>	x																						
F	Pelagic	<i>Cyclotella schumannii</i> (Grunow) Håkansson																							
F	Pelagic and epilithic	<i>Cymbella affinis</i> Kützing																							
B	Pelagic	<i>Diatoma moniliformis</i>	x			x				x															
F	Pelagic and pelagic	<i>Diatoma tenue</i>	x																						
BF	Pelagic	<i>Diatoma vulgare</i>																							
BF	Epipellic	<i>Diploneis smithii</i>	x																						
F	Pelagic and epilithic	<i>Encyonema silesiacum</i>	x			x																			
BF	Pelagic	<i>Epithemia sorex</i>	x																						
BF	Pelagic	<i>Epithemia turgida</i>					x																		
F		<i>Eunotia</i> cf. <i>septentrionalis</i>																							
F		<i>Eunotia implicata</i>	x	x																					
BM	Epipellic	<i>Fallacia pseudony</i> / <i>Fallacia oculiformis</i>	x																						
M		<i>Fragilaria capensis</i>	x																						
F		<i>Fragilaria exigua</i> Grunow	x	x																					
BF and SI		<i>Fragilariopsis cylindrus</i>																							
F		<i>Gomphocymbella anceli</i> (Cleve) Hustedt																							
F	Pelagic	<i>Gomphonema acuminatum</i> (Ehrenberg) W. Smith																							
F		<i>Gomphonema clavatum</i>	x																						
BF	Pelagic and epilithic	<i>Gomphonema olivaceum</i>																							
BF	Epipellic	<i>Gyrosigma acuminatum</i> (Kützing) Rabenhorst																							
F	Epipsammic	<i>Karayevia clevei</i>	x																						
B	Epipsammic	<i>Martyana schulzii</i>																							
BF	Epipellic and epilithic	<i>Mastogloia smithii</i>	x																						
BF	Epilithic and pelagic	<i>Melosira lineata</i> (Dillwyn) C.A. Agardh																							
		<i>Navicula bottanica</i>	x																						
BF		<i>Navicula cincta</i>	x																						
B		<i>Navicula halophila</i> (Grunow) Cleve																							
B	Epipellic	<i>Navicula peregrina</i>	x																						
		<i>Navicula psuedoscutiformis</i>	x																						
		<i>Navicula witkowskii</i>	x																						
B and SI	Pelagic	<i>Pauliella taeniata</i> (Grunow) Round and Basson	x	x	x																				
M	Epipellic	<i>Pinnularia cruciformis</i>	x																						
M		<i>Pinnularia quadratarea</i>																							
M		<i>Pinnularia</i> cf. <i>quadratarea</i> var. <i>subproducta</i> (Grunow) Cleve																							
F		<i>Pinnularia rostellata</i> Hustedt																							
M	Benthic	<i>Plagiogramma stauraphorum</i>																							
BF	Episammic and epilithic	<i>Planothidium delicatulum</i>																							
M?	Pelagic	<i>Pseudosolenia calcar-avis</i>																							
B	Pelagic and epilithic	<i>Rhoicosphenia curvata</i>	x	x	x																				
BF	Epipellic and epilithic	<i>Rhopalodia gibba</i>	x	x																					
F		<i>Stausirella lapponica</i>	x																						
F	Pelagic	<i>Stephanodiscus neoastraea</i>																							
BF	Epipellic and epilithic	<i>Surirella brebissonii</i> Krammer and Lange-Bertalot																							
F	Pelagic	<i>Synedra acus</i>																							
F	Pelagic	<i>Synedra ulna</i>	x																						
F	Epilithic and apiphytic	<i>Tabularia flocculosa</i>	x	x																					
B?		<i>Tabularia</i> cf. <i>laevis</i>																							
BM	Pelagic	<i>Tabularia fasciculata</i>	x																						

Table T2 (continued).

Affinity	Life form	Core, section, interval (cm): Diatoms	1H-1	2H-1	3H-1	3H-2	3H-CC	4H-1	4H-2	4H-3	6H-1	6H-2	7H-1, 77	7H-2, 2	7H-3, 2	8H-1	8H-2	9H-1	9H-2	9H-3	10H-1	10H-2	10H-3
									1 valve	Fragments	4 valves	Barren	Barren	Barren	Barren	Barren	2 valves	Barren	Barren	Barren	Barren	Barren	Barren
BF		<i>Tabularia tabulata</i> (C.A. Agard) Snoeijs			x		x																
BM	Pelagic	<i>Tabularia waernii</i>	x																				
BF	Pelagic	<i>Thalassiosira baltica</i>	x	x																			
B	Pelagic	<i>Thalassiosira hyperborea</i> var. <i>lacunosa</i>		x																			
F	Pelagic	<i>Thalassiosira lacustris</i>	x																				
B	Pelagic	<i>Thalassiosira levanderi</i>	x	x	x																		
BF	Epipelagic	<i>Tryblionella plana</i>						x															
		Silicoflagellates																					
		<i>Dictyocha speculum</i>																					
		Ebridians																					
		<i>Ebria tripartita</i>				x																	
		Crysohyte cysts																					
		Smooth	x	x	x	x	x	x															
		With spines						x															
		With curves		x	x																		
		Dots				x	x	x															
		Short ridges		x	x																		
		Tree hat						x															

F = freshwater, BF = brackish-freshwater, B = brackish, BM = brackish-marine, M = marine. x = present, c = common. ? = uncertain.



Table T3. Diatoms, Hole M0061B.

			Depth (mbsf):	2.80	4.30	5.80	6.10	7.59	9.09
			Core, section:	2H-1	2H-2	2H-3	3H-1	3H-2	3H-3
			Interval (cm):	0-1	0-1	0-1	0-1	0-1	0-1
Affinity	Life form	Diatoms							
BM		<i>Achnanthes brevipes</i> var. <i>intermedia</i> (Kützing) Cleve							x
F		<i>Achnanthes subatomides</i> (Hustedt) Lange-Bertalot and Archibald	x						
F	Epipellic and epilithic	<i>Amphora copulata</i>			x				
BF	Epipellic and epilithic	<i>Amphora pediculus</i>			x				
F		<i>Aulacoseira alpigena</i> (Grunow) Krammer	x						
F	Pelagic	<i>Aulacoseira islandica</i>			x				
F		<i>Aulacoseira subarctica</i> (O. Müller) Haworth				x			
F	Epipellic and epilithic	<i>Brachysira vitrea</i> (Grunow) Ross	x	x					
M/B	Pelagic	<i>Chaetoceros</i> resting spores spp.	c	c	c	c			
BF	Epiphytic and epilithic	<i>Cocconeis placentula</i>			x			x	
B	Epiphytic and episammic	<i>Cocconeis placentula</i> var. <i>euglypta</i> (Ehrenberg) Grunow	x						
B	Epiphytic	<i>Cocconeis scutellum</i>			x	x	x		
BM	Epiphytic	<i>Cocconeis stauroneiformis</i> (W. Smith) Okuno					x		
BF	Epiphytic	<i>Ctenophora pulchella</i> (Ralfs ex Kützing) Williams and Round				x			
B		<i>Cyclotella</i> cf. <i>caspia</i> Grunow	x						
B	Pelagic and epilithic	<i>Cyclotella choctawhatcheana</i>	x	x	x	x			
F		<i>Cyclotella stelligera</i> Cleve and Grunow	x	x					
B	Epiphytic	<i>Diatoma moniliformis</i>	x						
B	Epipellic	<i>Diploneis stroemii</i>	x						
F		<i>Encyonema minutum</i> (Hilse) D.G. Mann			x				
BF	Epiphytic	<i>Epithemia sorex</i>	x						
BF	Epiphytic	<i>Epithemia turgida</i>	x			x			
F		<i>Fragilaria exigua</i> Grunow	x						
SI		<i>Fragilariopsis cylindrus</i>	x						
BM	Epiphytic	<i>Gomphonemopsis exigua</i>			x				
B	Epipsammic	<i>Martyana schulzii</i>	x						
B arctic	Pelagic and ice	<i>Melosira</i> cf. <i>artica</i> Dickie			x				
B	Epilithic	<i>Navicula bottanica</i> Grunow					x		
F		<i>Navicula</i> cf. <i>impexa</i> Hustedt	x			x		x	
BF	Epipellic	<i>Navicula rhynocephala</i>	x	x	x				
M	Epipsammic	<i>Opephora marina</i>							x
B	Pelagic	<i>Pauliella taeniata</i> (Grunow) Round and Basson	c	c	x	x			
BM	Epipellic	<i>Petronis marina</i> (Ralfs) D.G. Mann					x		
M?	Pelagic	<i>Pseudosolenia calcar-avis</i>					x	x	
B	Epiphytic and epilithic	<i>Rhoicosphenia curvata</i>	x	x	x	x			
BF	Epipellic and epilithic	<i>Rhopalodia gibba</i>	x	x					
B	Pelagic	<i>Skeletonema costatum</i>	x						
F	Epilithic and apiphytic	<i>Tabelaria flocculosa</i>							x
BM	Epiphytic	<i>Tabularia fasciculata</i>	x	x	x	x			
BM	Pelagic	<i>Thalassionema nitzschioides</i>							x
BF	Pelagic	<i>Thalassiosira baltica</i>	x						
B	Pelagic	<i>Thalassiosira hyperborea</i> var. <i>lacunosa</i>	x	x	x	x			
BF	Pelagic	<i>Thalassiosira hyperborea</i> var. <i>pelagica</i> (Cleve-Euler) Hasle	x	x					
B	Pelagic	<i>Thalassiosira levanderi</i>	x	x	x	x			
M?	Pelagic	<i>Thalassiosira</i> sp.							x
Silicoflagellates									
		<i>Dictyocha speculum</i>							
Ebridians									
		<i>Ebria tripartita</i>	x	x					x
Crysophyte cysts									
		Smooth	x	x					
		With spines	x			x			
		With curves	x	x					
		Dots							
		Short ridges	x	x					x
		Tree hat							

F = freshwater, BF = brackish-freshwater, B = brackish, BM = brackish-marine, M = marine, SI = sea ice indicator. x = present, c = common. ? = uncertain.

Table T4. Species list of diatoms, Site M0061. (Continued on next page.)

Taxonomic list
Marine taxa
<i>Fragilaria capensis</i> Grunow
<i>Opephora marina</i> (Gregory) Petit
<i>Pinnularia</i> cf. <i>quadratarea</i> var. <i>subproducta</i> (Grunow) Cleve
<i>Pinnularia cruciformis</i> (Donkin) Cleve
<i>Pinnularia quadratarea</i> (A. Schmidt) Cleve
<i>Plagiogramma staurophorum</i> (W. Gregory) Heiberg
<i>Pseudosolenia calcar-avis</i> (Schultze) B.G. Sundström
<i>Thalassiosira</i> sp.
Brackish-marine taxa
<i>Achnanthes brevipes</i> var. <i>intermedia</i> (Kützing) Cleve
<i>Chaetoceros</i> resting spores spp.
<i>Cocconeis stauroneiformis</i> (W. Smith) Okuno
<i>Fallacia pseudony</i> (Hustedt) D.G. Mann
<i>Gomphonemopsis exigua</i> (Kützing) L.K. Medlin
<i>Petroneis marina</i> (Ralfs) D.G. Mann
<i>Tabularia fasciculata</i> (C. Agardh) D.M. Williams and Round
<i>Tabularia waernii</i> Snoeijis
<i>Thalassionema nitzschioides</i> (Grunow) Mereschkowsky
Brackish taxa
<i>Achnanthes leonardii</i> Witkowski and Lange-Bertalot
<i>Achnanthes lemmermannii</i> Hustedt
<i>Chamaepinnularia witkowskii</i> (H. Lange-Bertalot and D. Metzeltin) M. Kulikovskiy and H. Lange-Bertalot
<i>Cocconeis placentula</i> var. <i>euglypta</i> (Ehrenberg) Grunow
<i>Cocconeis scutellum</i> Ehrenberg
<i>Cyclotella</i> cf. <i>caspia</i> Grunow
<i>Cyclotella choctawhatcheeana</i> Prasad
<i>Cyclotella schumannii</i> (Grunow) Håkansson
<i>Diatoma moniliforme</i> (Kützing) D.M. Williams
<i>Diploneis stroemii</i> Hustedt
<i>Martyana schulzii</i> (Brockmann) Snoeijis
<i>Melosira</i> cf. <i>arctica</i> Dickie
<i>Navicula bottanica</i> Grunow
<i>Navicula halophila</i> (Grunow) Cleve
<i>Navicula peregrina</i> (Ehrenberg) Kützing
<i>Pauliella taeniata</i> (Grunow) Round and Basson
<i>Rhoicosphenia curvata</i> (Kützing) Grunow
<i>Skeletonema costatum</i> (Greville) Cleve
<i>Tabularia</i> cf. <i>laevis</i> Kützing
<i>Thalassiosira hyperborea</i> var. <i>lacunosa</i> Hasle
<i>Thalassiosira levanderi</i> Van Goor
Brackish-freshwater taxa
<i>Actinocyclus octonarius</i> var. <i>tenellus</i> (Brébisson) Hendeby
<i>Amphora pediculus</i> (Kützing) Grunow ex A. Schmidt
<i>Aneumastus minor</i> Lange-Bertalot
<i>Cavinula pseudoscutiformis</i> (Hustedt) D.G. Mann and A.J. Stickle
<i>Cocconeis pediculus</i> Ehrenberg
<i>Cocconeis placentula</i> Ehrenberg
<i>Ctenophora pulchella</i> (Ralfs ex Kützing) Williams and Round
<i>Cyclotella meneghiniana</i> Kützing
<i>Diatoma vulgare</i> Bory de Saint-Vincent
<i>Diploneis smithii</i> (Brébisson) Cleve
<i>Epithemia sorex</i> Kützing
<i>Epithemia turgida</i> (Ehrenberg) Kützing
<i>Fragilariopsis cylindrus</i> (Grunow) Krieger
<i>Gomphonema olivaceum</i> (Hornemann) Brébisson
<i>Gyrosigma acuminatum</i> (Kützing) Rabenhorst
<i>Mastogloia smithii</i> Thwaites ex W. Smith
<i>Melosira lineata</i> (Dillwyn) C.A. Agardh
<i>Navicula cincta</i> (Ehrenberg) Ralfs
<i>Navicula rhyncephala</i> Kützing
<i>Planothidium delicatulum</i> (Kützing) Round and Bukhtiyarova
<i>Rhopalodia gibba</i> (Ehrenberg) O. Müller
<i>Surirella brebissonii</i> Krammer and Lange-Bertalot
<i>Tabularia tabulata</i> (C.A. Agardh) Snoeijis
<i>Thalassiosira baltica</i> (Grunow) Ostenfeld
<i>Thalassiosira hyperborea</i> var. <i>pelagica</i> (Cleve-Euler) Hasle
<i>Tryblionella plana</i> (W. Smith) Pelletan

Table T4 (continued).

Taxonomic list
Freshwater taxa
<i>Achnanthes subatomides</i> (Hustedt) Lange-Bertalot and Archibald
<i>Amphora copulata</i> (Kützing) Schoeman and Archibald
<i>Aneumastus tusculus</i> (Ehrenberg) Mann and Stickle
<i>Aulacoseira alpigena</i> (Grunow) Krammer
<i>Aulacoseira ambigua</i> (Grunow) Simonsen
<i>Aulacoseira granulata</i> (Ehrenberg) Simonsen
<i>Aulacoseira subarctica</i> (O. Müller) Haworth
<i>Aulacoseira islandica</i> (O. Müller) Simonsen
<i>Brachysira vitrea</i> (Grunow) Ross
<i>Cocconeis disculus</i> (Schumann) Cleve
<i>Cyclotella atomus</i> Hustedt
<i>Cyclotella ocellata</i> Pantocsek
<i>Cyclotella radiosa</i> (Grunow) Lemmermann
<i>Cyclotella stelligera</i> Cleve and Grunow
<i>Cymbella affinis</i> Kützing
<i>Diatoma tenue</i> C.A. Agardh
<i>Encyonema minutum</i> (Hilse) D.G. Mann
<i>Encyonema silesiacum</i> (Bleisch) D.G. Mann
<i>Eunotia</i> cf. <i>septentrionalis</i> Østrup
<i>Eunotia implicata</i> Nörpel, Lange-Bertalot and Alles
<i>Fragilaria exigua</i> Grunow
<i>Gomphocymbella ancyli</i> (Cleve) Hustedt
<i>Gomphonema accuminatum</i> (Ehrenberg) W. Smith
<i>Gomphonema clavatum</i> Ehrenberg
<i>Karayevia clevei</i> (Grunow) Bukhtiyarova
<i>Navicula</i> cf. <i>impexa</i> Hustedt
<i>Pinnularia rostellata</i> Hustedt
<i>Stausosirella lapponica</i> (Grunow) D.M. Williams and Round
<i>Stephanodiscus neoastraea</i> Håkansson and Hickel
<i>Synedra acus</i> Kützing
<i>Synedra ulna</i> (Nitzsch) Ehrenberg
<i>Tabelaria flocculosa</i> (Roth) Kützing
<i>Thalassiosira lacustris</i> (Grunow) Hasle

Salinity affinities follows Snoeijs et al. (1993–1998). Diatom authorities according to AlgaeBase (www.algaebase.org).

Table T5. Foraminifers, Site M0061.

Hole, core, section, interval (cm)	Depth (mbsf)		Abundance	Number of species	<i>Elphidium albumbilicatum</i>
	Top	Bottom			
347-					
M0061B-1H-1, 77–79	0.00	0.02	B		
M0061B-1H-1, 17–19	0.17	0.19	B		
M0061A-1H-1, 40–42	0.40	0.42	B		
M0061A-1H-1, 131–133	1.31	1.33	B		
M0061A-1H-CC	1.38	1.53	B		
M0061C-1H-2, 4–6	1.54	1.56	B		
M0061B-1H-2, 17–19	1.67	1.69	V	1	x
M0061B-1H-CC	2.82	2.83	R	1	x
M0061B-2H-1, 15–17	2.95	2.97	B		
M0061A-2H-2, 18–20	3.18	3.20	V	1	x
M0061C-1H-CC	3.37	3.41	C	1	x
M0061B-2H-2, 15–17	4.45	4.47	R	1	x
M0061A-2H-CC	4.91	4.94	B		
M0061C-2H-2, 13–15	4.93	4.95	F	1	x
M0061A-3H-1, 30–32	5.10	5.12	V	1	x
M0061B-2H-CC	6.21	6.23	V	1	x
M0061C-2H-CC	6.70	6.72	B		
M0061C-3H-1, 15–17	6.75	6.77	B		
M0061B-3H-2, 13–15	7.72	7.74	B		
M0061A-3H-CC	8.05	8.08	B		
M0061B-3H-CC	9.53	9.54	B		
M0061A-4H-2, 15–17	9.75	9.77	B		
M0061C-3H-CC	10.02	10.04	B		
M0061C-4H-1, 15–17	10.05	10.07	B		
M0061A-4H-CC	11.25	11.28	B		
M0061B-4H-CC	12.40	12.55	B		
M0061A-6H-2, 15–17	12.85	12.87	B		
M0061C-4H-CC	13.02	13.04	B		
M0061A-6H-CC	13.26	13.33	B		
M0061B-5H-2, 15–17	14.35	14.37	B		
M0061C-5H-2, 15–17	14.85	14.87	B		
M0061B-5H-CC	15.84	15.87	B		
M0061A-7H-2, 12–14	16.12	16.14	B		
M0061B-6H-1, 18–20	16.18	16.20	B		
M0061C-5H-CC	16.52	16.57	B		
M0061A-7H-CC	17.66	17.68	B		
M0061A-8H-2, 15–17	19.25	19.27	B		
M0061B-6H-CC	19.29	19.30	B		
M0061B-7H-1, 24–26	19.54	19.56	B		
M0061C-6H-CC	19.65	19.72	B		
M0061A-8H-CC	20.74	20.77	B		
M0061A-9H-2, 15–17	22.45	22.47	B		
M0061B-7H-CC	22.48	22.51	B		
M0061C-7H-CC	22.95	22.97	B		
M0061A-9H-3		24.03	B		
M0061B-8H-1, 18–20	24.25	24.27	B		
M0061B-8H-CC	25.65	25.69	B		
M0061A-10H-2, 15–17	25.75	25.77	B		
M0061B-9H-2, 15–17	27.55	27.57	B		
M0061B-9H-CC	28.68	28.73	B		

Abundance: C = common, R = rare, B = barren, V = very high.

Table T6. Distribution and abundance of ostracods, Site M0061.

Core, section, interval (cm)	Depth (mbsf)	Overall abundance/20 cm ³	<i>Hirschmania viridis</i>	<i>Paracyprideis iennica</i>	<i>Heterocyprideis sorbyana</i>	<i>Sarsicytheridea punctillata</i>
347-M0061A-						
1H-1, 40–42	0.41	B				
1H-1, 131–133	1.32	R		R		
1H-CC, 0–15	1.38	B				
2H-2, 18–20	3.19	B				
2H-CC, 18–21	4.91	B				
3H-1, 30–32	5.11	R	R			
3H-CC, 25–28	8.05	B				
4H-2, 15–17	9.76	B				
4H-CC, 12–15	11.25	B				
6H-2, 15–17	12.86	B				
6H-CC, 0–7	13.26	B				
7H-2, 12–14	16.13	B				
7H-CC, 0–2	17.66	B				
8H-2, 15–17	19.26	B				
8H-CC, 0–3	20.74	B				
9H-2, 15–17	22.46	B				
9H-3, 22–23	24.02	B				
10H-2, 15–17	25.76	B				
347-M0061B-						
1H-1, 17–19	0.17	R		R		
1H-1, 77–79	1.67	R		R		
1H-CC, 13–14	2.82	C		F	R	R
2H-1, 15–17	2.95	F		F		
2H-2, 17–19	4.45	F		F		
2H-CC, 20–22	6.21	B				
3H-2, 13–15	7.72	B				
3H-CC, 23–24	9.53	B				
4H-CC, 0–15	12.40	B				
5H-2, 15–17	14.35	B				
5H-CC, 0–3	15.84	B				
7H-1, 24–26	16.18	B				
6H-CC, 10–11	19.29	B				
6H-1, 18–20	19.54	B				
7H-CC, 0–3	22.48	B				
8H-1, 18–20	24.25	B				
8H-CC, 4–8	25.65	B				
9H-2, 15–17	27.55	B				
9H-CC, 0–5	28.68	B				
347-M0061C-						
1H-2, 4–6	1.54	F		F		
1H-CC, 18–22	3.37	B				
2H-2, 13–15	4.93	B				
2H-CC, 19–21	6.70	B				
3H-1, 15–17	6.75	B				
3H-CC, 24–26	10.02	B				
4H-1, 15–17	10.05	B				
4H-CC, 0–2	13.02	B				
5H-2, 15–17	14.85	B				
5H-CC, 5–10	16.52	B				
6H-CC, 7–14	19.65	B				
7H-CC, 3–5	22.95	B				

Abundance: C = common, F = few, R = rare, B = barren.

Table T7. Calculated salinity and elemental ratios of interstitial waters, Site M0061.

Core, section, interval (cm)	Type	Depth (mbsf)	Cl ⁻ based salinity	Anion-based salinity	Na/Cl (mM/mM)	Ca/Cl (mM/mM)	Mg/Cl (mM/mM)	K/Cl (mM/mM)	Br/Cl (μM/mM)	B/Cl (μM/mM)
347-M0061A-										
1H-1, 123–128	Rh	1.23	6.11	7.34	0.82	0.02	0.09	0.02	1.57	1.01
2H-1, 135–140	Rh	2.85	6.79	9.64	0.82	0.03	0.10	0.02	1.65	1.21
2H-2, 135–140	Rh	4.35	7.18	11.53	0.84	0.03	0.10	0.02	1.67	1.21
3H-1, 135–140	Rh	6.15	7.70	13.85	0.82	0.04	0.10	0.02	1.62	0.94
3H-2, 135–140	Rh	7.65	8.00	15.65	0.80	0.04	0.10	0.02	1.64	0.70
4H-1, 135–140	Rh	9.45	8.09	17.54	0.78	0.05	0.09	0.02	1.63	0.52
4H-2, 64–69	Rh	10.24	8.20	18.44	0.77	0.06	0.09	0.01	1.62	0.42
6H-1, 135–140	Rh	12.55	8.24	20.79	0.73	0.07	0.08	0.01	1.61	0.21
7H-1, 135–140	Rh	15.85	7.98	23.83	0.67	0.10	0.08	0.01	1.61	0.06
7H-2, 75–80	Rh	16.75	7.94	24.69	0.66	0.10	0.08	0.01	1.60	0.03
8H-1, 135–140	Rh	18.95	7.96	26.91	0.71	0.12	0.09	0.01	1.61	0.00
8H-2, 75–80	Rh	19.85	8.02	27.87	0.63	0.11	0.08	0.01	1.61	0.00
9H-1, 135–140	Rh	22.15	8.28	30.43	0.63	0.13	0.10	0.01	1.59	0.00
10H-1, 135–140	Rh	25.45	8.32	33.77	0.58	0.13	0.09	0.01	1.53	0.00
347-M0061B-										
1H-1, 135–140	Rh	1.35	6.12	7.47	0.83	0.02	0.10	0.02	1.60	0.99
1H-2, 104–109	Rh	2.54	6.52	9.06	0.92	0.03	0.12	0.02	1.63	1.31
2H-1, 135–140	Rh	4.15	7.12	11.27	0.86	0.03	0.11	0.02	1.64	1.23
2H-2, 135–140	Rh	5.65	7.52	13.17	0.82	0.04	0.10	0.02	1.66	1.03
3H-1, 134–139	Rh	7.44	7.87	15.31	0.83	0.04	0.10	0.02	1.63	0.76
3H-2, 135–140	Rh	8.94	8.09	17.03	0.80	0.05	0.10	0.02	1.62	0.58
4H-1, 135–140	Rh	10.75	8.17	18.92	0.73	0.07	0.08	0.01	1.61	0.23
4H-2, 135–140	Rh	12.25	8.16	20.41	0.77	0.06	0.09	0.01	1.61	0.36
5H-1, 135–140	Rh	14.05	8.06	22.11	0.71	0.08	0.08	0.01	1.60	0.15
5H-2, 135–140	Rh	15.55	8.05	23.60	0.69	0.09	0.08	0.01	1.60	0.08
6H-1, 135–140	Rh	17.35	8.00	25.35	0.66	0.10	0.08	0.01	1.60	0.04
6H-2, 135–140	Rh	18.85	8.09	26.94	0.65	0.11	0.08	0.01	1.60	0.02
7H-1, 135–140	Rh	20.65	8.25	28.90	0.62	0.12	0.09	0.01	1.59	0.00
7H-2, 135–140	Rh	22.15	8.44	30.59	0.60	0.13	0.09	0.01	1.58	0.00
8H-1, 135–140	Rh	23.95	8.62	32.57	0.57	0.15	0.10	0.01	1.57	0.00
9H-1, 135–140	Rh	27.25	9.22	36.47	0.52	0.16	0.10	0.01	1.55	0.00
347-M0061C-										
1H-1, 135–140	Rh	1.35	6.22	7.57	0.80	0.02	0.09	0.02	1.61	0.99
1H-2, 135–140	Rh	2.85	6.58	9.43	0.82	0.03	0.10	0.02	1.64	1.22
2H-1, 135–140	Rh	4.65	7.42	12.07	0.99	0.04	0.13	0.03	1.64	1.44
2H-2, 135–140	Rh	6.15	7.51	13.66	0.92	0.04	0.12	0.02	1.64	1.16
3H-1, 135–140	Rh	9.45	7.59	17.04	0.91	0.05	0.11	0.02	1.62	1.00
4H-1, 135–140	Rh	11.25	7.85	19.10	0.92	0.10	0.12	0.02	1.59	0.50
4H-2, 125–130	Rh	12.65	7.81	20.46	0.87	0.13	0.12	0.02	1.58	0.30
5H-1, 135–140	Rh	14.55	7.71	22.26	0.77	0.15	0.12	0.01	1.58	0.16
5H-2, 135–140	Rh	16.05	7.78	23.83	0.72	0.16	0.12	0.01	1.59	0.11
6H-1, 135–140	Rh	17.85	7.76	25.61	0.71	0.20	0.14	0.01	1.58	0.05
6H-2, 125–130	Rh	19.25	7.80	27.05	0.55	0.16	0.11	0.01	1.58	0.02
7H-1, 135–140	Rh	21.15	7.90	29.05	0.59	0.21	0.13	0.01	1.57	0.02

Rh = Rhizon sample.

Table T8. Interstitial water geochemistry, Site M0061.

Core, section, interval (cm)	Type	Depth (mbsf)	Volume (mL)	Analyte:	pH	Salinity	Alkalinity	Cl ⁻	Br ⁻	SO ₄ ²⁻	H ₂ S	NH ₄ ⁺	Na ⁺	K ⁺	Mg ²⁺	Ca ²⁺	Sr ²⁺	Li ⁺	H ₄ SiO ₄	Ba ²⁺	B	Al	PO ₄ ³⁻	Fe ²⁺	Mn ²⁺	Mo	Ti	V	Zr		
				Unit:	ISE	Refraction	meq/L	mM	mM	mM	mM	mM	mM	mM	mM	mM	mM	mM	mM	mM	mM	mM	mM	mM	mM	mM	mM	mM	mM	mM	mM
				Method:	IC	IC	Titration	IC	IC	IC	Photometric	Conductivity	ICP-OES	ICP-OES	ICP-OES	ICP-OES	ICP-OES	ICP-OES	ICP-OES	ICP-OES	ICP-OES	ICP-OES	ICP-OES	ICP-OES	ICP-OES	ICP-OES	ICP-OES	ICP-OES	ICP-OES	ICP-OES	
347-M0061A-																															
1H-1, 123-128	Rh	1.23	26.0		7.92	6.40	13.49	97.35	0.15	0.03	0.00	0.51	80.30	2.19	9.18	2.29	16.22	4.60	695.03	0.42	98.05	0.89	0.38	94.62	253.01	0.04	0.23	0.18	0.04		
2H-1, 135-140	Rh	2.85	24.0		7.81	6.40	14.47	108.22	0.18	0.17	0.00	1.11	89.26	2.46	11.07	2.98	20.22	7.55	713.90	0.58	131.07	0.67	0.54	50.84	164.66	0.04	0.10	0.11	0.02		
2H-2, 135-140	Rh	4.35	13.0		7.93	7.80	19.24	114.41	0.19	0.02	0.01	1.30	95.87	2.53	11.98	3.58	21.25	8.17	725.65	2.06	138.56	1.11	0.51	6.70	47.11	0.03	0.05	0.10	0.01		
3H-1, 135-140	Rh	6.15	6.0		8.11	8.20	19.49	122.81	0.20	0.25	0.00	1.23	100.39	2.42	12.06	4.45	21.84	5.96	670.11	6.47	115.44	0.52	0.28	23.64	51.95	0.06	0.04	0.10	0.02		
3H-2, 135-140	Rh	7.65	48.0		7.65	8.40	19.43	127.62	0.21	0.07	0.00	1.12	102.09	2.29	12.21	5.21	21.43	3.56	603.88	9.09	89.72	0.52	0.10	317.66	55.90	0.04	0.00	0.02	0.01		
4H-1, 135-140	Rh	9.45	19.0		7.72	8.20	17.63	128.91	0.21	0.07	0.00	0.96	100.13	2.03	11.36	6.55	21.81	3.07	354.32	12.18	67.52	0.89	0.04	359.92	63.27	0.04	0.01	0.06	0.01		
4H-2, 64-69	Rh	10.24	35.0		7.67	8.40	17.36	130.68	0.21	0.14	0.00	0.88	100.09	1.94	11.35	7.33	22.55	3.63	318.00	12.85	55.22	0.48	0.03	328.95	71.61	0.09	0.00	0.04	0.01		
6H-1, 135-140	Rh	12.55	36.0		7.69	8.20	14.06	131.42	0.21	0.25	0.00	0.73	96.09	1.79	10.97	9.80	25.19	7.13	327.08	13.82	28.03	0.82	0.01	362.61	110.63	0.17	0.00	0.06	0.01		
7H-1, 135-140	Rh	15.85	18.0		7.68	7.60	11.34	127.23	0.21	0.11	0.00	0.49	85.17	1.26	10.00	12.10	28.04	6.36	318.57	13.74	8.14	0.48	0.01	264.30	127.51	0.07	0.01	0.08	0.00		
7H-2, 75-80	Rh	16.75	41.0		7.73	7.60	10.98	126.52	0.20	0.10	0.00	0.47	83.51	1.27	10.00	12.51	28.77	6.72	309.85	14.70	3.88	0.26	0.00	209.15	114.78	0.14	0.00	0.08	0.00		
8H-1, 135-140	Rh	18.95	40.0		7.67	7.70	10.93	126.95	0.20	0.02	0.00	0.44	90.08	1.21	11.80	15.54	35.77	6.75	358.91	15.33	0.00	0.44	0.01	253.56	111.62	0.08	0.00	0.06	0.00		
8H-2, 75-80	Rh	19.85	42.0		7.61	7.90	10.57	127.87	0.21	0.01	0.00	0.41	80.73	1.11	10.52	13.86	32.17	7.17	313.80	13.19	0.00	0.44	0.00	191.42	88.88	0.07	0.00	0.06	0.00		
9H-1, 135-140	Rh	22.15	37.0		7.74	8.00	9.76	132.04	0.21	0.55	0.00	0.37	83.38	1.16	12.83	17.42	42.20	8.11	358.55	14.04	0.00	0.44	0.00	110.32	77.94	0.04	0.00	0.07	0.02		
10H-1, 135-140	Rh	25.45	42.0		7.74	8.80	8.97	132.60	0.20	1.45	0.00	0.35	77.56	1.24	12.40	17.51	43.19	9.12	319.71	10.78	0.00	0.30	0.00	123.11	74.34	0.13	0.00	0.07	0.00		
347-M0061B-																															
1H-1, 135-140	Rh	1.35	38.0		7.75	6.30	13.46	97.50	0.16	0.03	—	0.64	80.64	2.14	9.45	2.34	16.47	4.69	693.61	0.42	96.57	1.07	0.39	87.90	266.48	0.10	0.21	0.16	0.03		
1H-2, 104-109	Rh	2.54	22.0		7.81	7.00	17.20	103.94	0.17	0.01	—	0.94	95.82	2.49	12.57	3.26	22.35	6.73	824.28	0.57	135.97	0.59	0.62	125.11	250.28	0.03	0.11	0.10	0.02		
2H-1, 135-140	Rh	4.15	15.0		7.90	7.50	19.70	113.54	0.19	0.10	—	1.28	97.17	2.57	12.41	3.69	22.10	8.11	739.18	2.16	139.95	2.08	0.52	5.89	50.93	0.04	0.06	0.10	0.02		
2H-2, 135-140	Rh	5.65	12.0		7.95	7.90	20.28	119.89	0.20	0.02	—	1.30	98.13	2.43	12.29	4.25	21.50	6.93	701.80	5.06	123.30	2.22	0.37	3.81	45.94	0.03	0.04	0.06	0.01		
3H-1, 134-139	Rh	7.44	16.0		7.91	7.70	19.57	125.43	0.20	0.02	—	1.23	104.52	2.30	12.95	5.47	22.88	3.72	670.82	9.34	94.81	2.04	0.15	319.46	59.14	0.00	0.01	0.04	0.01		
3H-2, 135-140	Rh	8.94	24.0		7.65	8.10	17.88	128.96	0.21	0.01	—	1.09	103.00	2.09	12.32	6.50	22.76	2.81	415.52	11.87	74.83	0.89	0.07	476.68	60.81	0.03	0.00	0.05	0.01		
4H-1, 135-140	Rh	10.75	45.0		7.57	8.10	15.86	130.24	0.21	0.03	—	0.87	94.61	1.59	10.93	9.40	24.40	5.14	344.63	13.41	30.25	1.00	0.01	344.35	109.31	0.12	0.01	0.05	0.01		
4H-2, 135-140	Rh	12.25	38.0		7.47	8.10	16.24	130.14	0.21	0.04	—	0.68	100.26	1.79	11.65	8.27	23.91	4.08	328.93	13.19	47.45	0.59	0.03	385.17	85.06	0.10	0.00	0.04	0.01		
5H-1, 135-140	Rh	14.05	40.0		7.67	7.70	18.67	128.55	0.21	0.02	—	0.61	90.65	1.39	10.49	10.49	25.72	5.21	334.95	13.92	19.24	0.52	0.01	303.16	124.72	0.08	0.00	0.00	0.00		
5H-2, 135-140	Rh	15.55	40.0		7.76	7.50	12.54	128.32	0.21	0.00	—	0.54	88.78	1.35	10.66	11.99	28.24	5.82	324.34	15.59	10.82	0.41	0.01	252.66	123.78	0.09	0.00	0.08	0.00		
6H-1, 135-140	Rh	17.35	42.0		7.74	7.40	10.44	127.60	0.20	0.03	—	0.50	84.65	1.21	10.45	12.80	30.19	5.85	329.14	14.24	4.53	0.26	0.01	256.07	100.73	0.08	0.00	0.09	0.00		
6H-2, 135-140	Rh	18.85	40.0		7.82	7.50	10.27	128.99	0.21	0.02	—	0.46	83.21	1.19	10.72	13.75	33.15	6.03	323.66	14.33	2.22	0.74	0.01	216.31	85.93	0.06	0.00	0.07	0.00		
7H-1, 135-140	Rh	20.65	40.0		7.99	7.80	9.73	131.48	0.21	0.02	—	0.42	81.12	1.21	11.40	15.45	39.33	7.45	342.28	14.08	0.00	0.37	0.00	77.39	71.44	0.03	0.00	0.10	0.04		
7H-2, 135-140	Rh	22.15	40.0		7.87	8.00	8.83	134.58	0.21	0.69	—	0.39	80.30	1.29	12.32	17.27	44.94	8.40	345.06	11.83	0.00	0.37	0.00	62.57	74.63	0.09	0.01	0.09	0.02		
8H-1, 135-140	Rh	23.95	40.0		7.77	8.30	7.11	137.42	0.22	2.00	—	0.33	77.69	1.32	13.27	20.00	52.88	8.61	330.14	4.42	0.00	0.48	0.00	102.01	72.03	0.04	0.00	0.11	0.00		
9H-1, 135-140	Rh	27.25	40.0		7.70	10.30	5.91	146.94	0.23	3.79	—	0.24	76.56	1.54	14.57	23.95	68.07	10.17	285.85	1.33	0.00	0.96	0.00	73.72	63.13	0.06	0.00	0.10	0.02		
347-M0061C-																															
1H-1, 135-140	Rh	1.35	33.0		7.79	6.87	15.26	99.19	0.16	0.05	0.00	0.60	78.95	2.11	9.15	2.28	16.16	5.58	700.37	0.39	98.60	2.67	0.39	83.25	249.74	0.01	0.23	0.17	0.09		
1H-2, 135-140	Rh	2.85	12.0		8.01	7.57	17.31	104.96	0.17	0.03	0.00	0.93	85.99	2.33	10.69	2.89	19.62	8.06	719.60	0.54	128.02	1.67	0.55	63.23	172.23	0.02	0.13	0.10	0.04		
2H-1, 135-140	Rh	4.65	8.0		8.23	8.48	18.53	118.23	0.19	0.24	0.00	1.23	116.83	2.99	15.37	4.74	27.52	8.62	875.56	3.47	170.20	4.15	0.57	7.18	47.34	0.00	0.06	0.10	0.00		
2H-2, 135-140	Rh	6.15	7.0		8.23	8.59	18.64	119.65	0.20	0.08	0.00	1.18	110.44	2.68	13.89	5.16	25.50	7.00	789.75	6.66	138.84	2.04	0.35	18.25	57.95	0.00	0.03	0.07	0.00		
3H-1, 135-140	Rh	9.45	14.0		8.08	8.80	18.12	120.96	0.20	0.14	0.00	1.15	110.27	2.64	13.29	5.51	24.91	5.54	798.29	8.43	121.27	3.34	0.23	149.02	61.96	0.00	0.04	0.09	0.00		
4H-1, 135-140	Rh	11.25	19.0		7.73	9.02	13.52																								

Table T9. Total carbon (TC), total organic carbon (TOC), total inorganic carbon (TIC), and total sulfur (TS) in sediment, Site M0061.

Core, section, interval (cm)	Depth (mbsf)	TC (wt%)	TOC (wt%)	TIC (wt%)	TS (wt%)
347-M0061A-					
1H-1, 74–75	0.74	1.43	1.34	0.09	0.68
2H-1, 64–65	2.14	1.83	1.73	0.09	1.32
3H-1, 27–28	5.07	2.13	2.06	0.07	1.97
4H-1, 35–36.5	8.45	0.75	0.71	0.05	0.10
4H-3, 50–51.5	10.89	0.27	0.23	0.04	0.10
6H-1, 61.5–63	11.82	0.23	0.20	0.04	0.13
7H-1, 70–71	15.20	0.14	0.09	0.05	0.13
7H-2, 57–58	16.57	0.18	0.12	0.06	0.13
8H-1, 55–56.5	18.15	0.17	0.11	0.06	0.16
9H-1, 104–105	21.84	0.14	0.09	0.05	0.14
9H-2, 144–145	23.74	0.10	0.09	0.01	0.11
10H-1, 144.5–146	24.49	0.16	0.10	0.06	0.13
10H-2, 101–102	27.05	0.12	0.06	0.06	0.12
347-M0061B-					
2H-2, 31–32	3.81	2.29	2.18	0.11	1.21
2H-1, 27–34	4.61	2.61	2.53	0.08	2.25
3H-1, 30–31	6.40	1.58	1.46	0.12	0.90
3H-1, 83–84	8.42	0.90	0.84	0.05	0.14
5H-1, 18–19	12.88	0.14	0.11	0.04	0.12
5H-2, 70–71	14.90	0.15	0.11	0.04	0.14
6H-1, 71–72	16.71	0.13	0.09	0.04	0.13
7H-1, 37–38	19.67	0.10	0.08	0.02	0.12
7H-2, 37–38	21.17	0.12	0.10	0.01	0.12
8H-1, 52–53	23.12	0.09	0.08	0.02	0.12
8H-2, 123–124	25.33	0.10	0.06	0.03	0.13
9H-1, 34–35	26.24	0.10	0.06	0.04	0.13
347-M0061C-					
1H-1, 83–84	0.83	1.59	1.43	0.16	0.54
1H-2, 41–42	1.91	1.52	1.36	0.16	0.70
2H-1, 39–40	3.69	2.35	2.13	0.21	1.37
3H-1, 97–98	7.57	1.56	1.46	0.10	0.87
3H-2, 97–98	9.07	0.59	0.53	0.07	0.09
3H-3, 7–8	9.67	0.74	0.72	0.02	0.10
5H-1, 44.5–46	13.65	0.18	0.13	0.05	0.13
6H-1, 73–74	17.23	0.15	0.10	0.06	0.16
7H-1, 70–71	20.50	0.17	0.11	0.06	0.12

Table T10. Samples taken for cell counts by acridine orange direct count (AODC), Hole M0061K.

Core, section, interval (cm)	Top depth (mbsf)	AODC (log cells/cm ³)
347-M0061K-		
1L-1	0.01	9.53
1L-1, 3	0.04	9.73
1L-1, 11	0.12	9.49
1L-1, 19	0.20	9.49
1L-1, 27	0.28	9.27
1L-1, 35	0.36	9.37
1L-1, 43	0.44	9.12
1L-1, 51	0.52	9.10
1L-1, 59	0.60	9.16
1L-1, 67	0.68	9.00
1L-1, 75	0.76	8.86
1L-1, 83	0.84	8.86
1L-1, 91	0.92	8.84

Count data are presented in logarithmic format.

Table T11. Composite depth scale, Site M0061.

Core	Offset (m)	Top depth	
		(mbsf)	(mcd)
347-M0061A-			
1H	-0.13	0	-0.13
2H	0.13	1.5	1.63
3H	0.20	4.8	5.00
4H	0.32	8.1	8.42
5H	0.32		0.32
6H	0.32	11.2	11.52
7H	0.10	14.5	14.60
8H	0.01	17.6	17.61
9H	0.01	20.8	20.81
10H	0.36	24.1	24.46
347-M0061B-			
1H	0.13	0	0.13
2H	0.06	2.8	2.86
3H	0.25	6.1	6.35
4H	-0.13	9.4	9.27
5H	-0.13	12.7	12.57
6H	-0.13	16	15.87
7H	-0.13	19.3	19.17
8H	0.03	22.6	22.63
9H	0.03	25.9	25.93
347-M0061C-			
1H	0.00	0	0.00
2H	0.00	3.3	3.30
3H	0.38	6.6	6.98
4H	0.10	9.9	10.00
5H	-0.19	13.2	13.01
6H	-0.38	16.5	16.12
7H	-0.57	19.8	19.23

Table T12. Splice tie points, Site M0061.

Hole, core, section, interval (cm)	Depth (mbsf)	Depth (mcd)		Hole, core, section, interval (cm)
347-				347-
M0061C-1H-2, 147	2.85	2.98	Tie to	M0061A-2H-1, 134
M0061A-2H-2, 80	3.93	3.93	Tie to	M0061C-2H-1, 63
M0061C-2H-2, 128	5.89	6.09	Tie to	M0061A-3H-1, 109
M0061A-3H-2, 111	7.36	7.61	Tie to	M0061B-3H-1, 126
M0061B-3H-2, 126	8.79	9.11	Tie to	M0061A-4H-1, 68
M0061A-4H-3, 8	10.70	10.80	Tie to	M0061C-4H-1, 80
M0061C-4H-2, 114	12.32	12.64	Tie to	M0061A-6H-1, 111
M0061A-6H-2, 23	13.38	13.25	Tie to	M0061B-5H-1, 68
M0061B-5H-2, 26	14.52	14.33	Tie to	M0061C-5H-1, 132
M0061C-5H-2, 106	15.47	15.57	Tie to	M0061A-7H-1, 96
M0061A-7H-3, 18	17.58	17.19	Tie to	M0061C-6H-1, 107
M0061C-6H-2, 107	18.69	18.69	Tie to	M0061A-8H-1, 108
M0061A-8H-3, 40	20.99	20.41	Tie to	M0061C-7H-1, 118
M0061C-7H-2, 137	22.09	22.10	Tie to	M0061A-9H-1, 128
M0061A-9H-2, 115	23.44	23.47	Tie to	M0061B-8H-1, 83
M0061B-8H-2, 96	24.73	25.09	Tie to	M0061A-10H-1, 62
M0061A-10H-2, 60	26.54	26.57	Tie to	M0061B-9H-1, 64

Table T13. Sound velocity data for lithologic units, Site M0061.

Unit	Thickness of unit (m)	Sound velocity (m/s)*	TWT (ms)	Depth (m)	Depth (mbsf)
Water	86	1430	0.1203	86	0
I	2.3	1472	0.1234	88.3	2.3
II	5.8	1472	0.1313	94.1	8.1
III	6.4	1472	0.1400	100.5	14.5
IV	14.2	1461	0.1594	114.7	28.7

* = sound velocities are based on values measured during the OSP. TWT = two-way traveltime.